Biosystems Engineering 245 (2024) 199–222

Contents lists available at ScienceDirect

Biosystems Engineering

journal homepage: www.elsevier.com/locate/issn/15375110

Research Paper

Modelling the interaction of soil with a passively-vibrating sweep using the discrete element method

Kornél Tamás

Department of Machine and Product Design, Faculty of Mechanical Engineering, Budapest University of Technology and Economics, Műegyetem rkp. 3., H-1111, Budapest, Hungary

ARTICLE INFO

Keywords:
Vibration dynamic
Kinetic energy
Genetic algorithm
Fast fourier transform
Soil bin test
Direct shear box test

ABSTRACT

This study investigates the passive vibration dynamics of a sweep tool in a laboratory soil bin test, employing various spring configurations. A discrete element method (DEM) model of simulating the passively vibrating sweep tool was developed based on the laboratory soil bin tests. Ensuring precision in the DEM model parameters was achieved by applying a genetic algorithm tailored for this purpose. The genetic algorithm revealed that within the particle assemblies of the three geometries used in the DEM, several parameter sets were suitable for accurately describing the modelled soil. The final parameter set was chosen by integrating the DEM model with results from the laboratory direct shear box test. Employing Fast Fourier Transformation, both the laboratory soil bin test and the calibrated DEM model of the soil and the vibrating sweep tool facilitated an examination of frequencies and amplitudes during force and displacement measurements. The results indicated that, compared to a rigid tool, the draught force required by the 16 spring sweep tool was reduced by 6–9%. The absence of DEM would have limited the investigation of kinetic energy in the sweep tool and the dynamics of energy dissipation in the soil, if measurement equipment alone was used. This research successfully demonstrated that the reduced draught force with the 16 spring passively vibrating sweep tool, operating near the system's eigenfrequency, resulted from its ability to generate higher kinetic energy in the sweep tool while minimising energy dissipation in the soil.

NOMENCLATURE

F	load force in the ringing test (N)
I_{sweep}	mass moment of inertia tensor (kg m^2)
R	the centre of mass of the sweep tool (m)
f_d	occurring frequency (Hz)
T_d	periodic time (s)
ω_d	eigenfrequency (s^{-1})
$\Lambda_{measured}$	logarithmic decrement in measurement
$\Lambda_{simulated}$	logarithmic decrement in simulation
A	amplitude (mm)
$\zeta_{measured}$	damping factor in the measurement
$\zeta_{simulated}$	damping factor in the simulation
E_k	total kinetic energy (J)
N_b	number of bodies
m_b	mass of a single body (kg)
v_b	translational velocity of a single body (m s^{-1})
I_b	mass moment of inertia of a single body (kg m^2)
ω_b	angular velocity of a single body (rad s^{-1})
RE_{freq}	relative error in frequency (%)
RE_{damp}	relative error in damping (%)
$freq_{sim}$	simulated frequency (Hz)
$freq_{target}$	measured frequency (Hz)
$damp_{sim}$	simulated damping
$damp_{target}$	measured damping
$RE_{Draught}$	relative error in draught (%)
$Draught_{sim}$	simulated mean draught (N)
$Draught_{target}$	measured mean draught (N)
ABBREVIATIONS	
DEM	Discrete Element Method
GA	Genetic Algorithm
FFT	Fast Fourier Transform
STL	Standard Tessellation Language
DoF	Degree of Freedom
GPU	Graphics Processing Unit

(*continued on next column*)

1. Introduction

The energy consumption associated with soil tillage involves significant costs, primarily due to the fuel consumption of the powered machines currently in use. Therefore, reducing the power consumption of

E-mail address: tamas.kornel@gt3.bme.hu.

https://doi.org/10.1016/j.biosystemseng.2024.06.006
Received 21 March 2024; Received in revised form 25 May 2024; Accepted 10 June 2024
Available online 31 July 2024
1537-5110/

these tillage tools is a critical concern today. Especially in arid periods, prioritising methods that do not involve rotation of the soil is essential. One of the recommended approaches is the use of sweep tools in conservation tillage methods. Although this method requires less power and consequently costs less than ploughing, further investigation into reducing the energy demand of sweep tools is crucial.

In the realm of soil tillage, a promising avenue of exploration involves the use of vibration-based tillage tools. This concept was first explored by Gunn and Tramontini (1955) whose research revealed that actively vibrated tools with an external energy input exert 60% less draught force and result in superior soil shredding compared to rigid tools. However, despite these advantages, the overall energy demand for the tillage process remained relatively stable due to the additional expenditure of energy required for vibration. Subsequent studies in the field of actively vibrated tillage tools with significant lower draught force further explored this phenomenon (Dubrovskij, 1956). This observation was the focal point of the work of Eggenmüller (1958), in which throwing the soil upward reduced the draught force required, which established that lower vibration frequencies were optimal for quality enhancement. Moreover, when amplitudes were lower, there was a 75% reduction in the draught force required during actively vibrating tillage. A similar result was obtained by Hendrick and Buchele (1963), which achieved a remarkable 90% reduction in the required draught force, emphasising that the optimal vibration depended on the soil's physical properties and the speed of the tractor. Various researchers have sought to determine the optimal parameters for actively vibrated tillage tools, and have universally agreed on the significance of frequency and amplitude of the vibrated tool (Kofoed, 1969; Shahgoli et al., 2010; Xirui et al., 2016). The research of Sulatisky and Ukrainetz (1972) revealed a correlation between a higher investment of power in vibration and greater reduction in the draught force required. They achieved an 80% draught force reduction, corroborating the findings of Yow and Smith (1976) and Bandalan et al. (1999), especially at a frequency of 10 Hz. However, this came at the cost of the entire system's power consumption increasing in comparison to rigid tools.

From the aforementioned studies, it becomes evident that active vibrated tillage tools are able to significantly reduce the draught force requirements for tillage and enhance soil quality. However, these advantages do not translate into decreased energy consumption, and thus fail to reduce fuel consumption during the loosening process. To address this limitation, researchers have explored an alternative approach involving unpowered, "passive" vibration mechanisms in tools, where the soil failure creates the oscillatory motion of the tillage tool.

Passively vibrated ploughs and sweep tools were investigated in the research of Fenyvesi and Hudoba (2010). They found that the optimal vibration in the moving direction of a passively vibrated tillage tool was at a frequency of 25–30 Hz, which lowered the energy requirements by 5–9% compared to rigid tools. It is worth noting, however, that their study did not develop a model to predict this reduction in draught force. Soeharsono and Setiawan (2010) utilised, Fourier Series analysis in their study, improving the analytical model for predicting draught force using vibratory tillage dynamics. Their simulation model was not capable of capturing soil quality changes arising due to the vibratory tool. Other researchers have found that increasing the tool's operation speed leads to higher frequency and amplitude in the passively vibrating tillage tool (Dzhabborov et al., 2021), but these results were not compared in most cases with measurements from rigid tools.

While extensive research has been conducted using laboratory and field tests and analytical models, ongoing investigations are exploring numerical methods, such as the finite element method (FEM) and the discrete element method (DEM). These numerical approaches are promising for further understanding and optimising the dynamics of vibrated tillage tools.

In Oladapo's (1993) study, the effect of a plough's natural frequency on tillage forces in sandy loam soil was investigated using a FEM model. While the computer-predicted results aligned well with the experimental data, further improvement with a more detailed simulation model was deemed necessary. Similarly, Zhang (1997) developed a FEM model and suggested that for self-excited oscillatory operation, future investigations should consider the effects of amplitude and frequency on the aggregate size of the soil. Additionally, Zhang (1997) recommended employing a more sophisticated model to describe the motion of the tillage tool.

The DEM was used in the research of Van der Linde (2007), which demonstrated that the effect of actively vibrated tillage tools on draught force reduction could be accurately simulated using DEM. It is worth emphasising that this work focused on active tools, and did not investigate passive tools. In a separate study by Keppler et al. (2015), DEM was utilised to model draught force reduction with passively vibrated sweep tools. However, their DEM model employed only harmonic vibration motion with infinite energy and lacked damping. This approach influenced the nature of the actively vibrated tillage tool mechanism. This research highlighted the need for improvement in DEM modelling, particularly for passive vibrated sweep tools. Future studies should focus on developing a suitable DEM model for simulating freely vibrated sweep tool geometries without relying on harmonic vibration motion engines. This improvement is necessary in order to accurately represent vibrations generated by both the soil and the sweep tool, which could be specifically tailored for passive vibration, and should be a focal point for further investigations. Both of the previously listed DEM models have been calibrated manually, which has the limitation to allow all applicable parameter combinations to be found for the model calibration.

In the research of Pásthy et al. (2024) a two-way coupled simulation procedure combining the DEM and the FEM for the modelling of passively vibrating tools was improved, however they proposed the application of calibration procedures aided by artificial intelligence and the measuring and simulating of the passive vibration of the tool in a longer soil bin and in the case of more complex tool geometry.

Based on the limited number of relevant studies in this field and the lack of a simulation model that agriculture engineers can use to design passively vibrated tools, it is evident that investigating the interaction between the soil and a passively vibrated sweep tools holds significant research potential.

To address the gaps identified in previous studies, this research aims to achieve the following objectives. It aims to conduct comprehensive experiments using a passively vibrated sweep tool to analyse the impact of the resulting frequencies, damping effects, and amplitudes under different spring stiffness settings in a controlled environment. It also seeks to enhance the DEM model and calibrate it using a genetic algorithm (GA) to accurately capture the vibration characteristics of the passively vibrated sweep tool. This calibration process will involve using ringing tests to refine the model. Moreover, the research will attempt to develop an advanced DEM model to simulate the interaction between the soil and the passively vibrated sweep tool. This simulation will provide insights into the dynamic behaviour of the system. It will also investigate the frequencies and amplitudes resulting from both laboratory tests and simulations, while utilising Fast Fourier Transform (FFT) methods to analyse the data, enabling a detailed frequency and amplitude analysis of the passively vibrated sweep tool's behaviour. This will allow the exploration of the reasons behind the reduction in the draught force requirements that have been observed in studies of passively vibrated sweep tools. The research will investigate the formation of kinetic energy in the passively vibrated sweep tool and the soil particle assembly. It will explore how different spring settings affect the distribution and transformation of kinetic energy within the system. By addressing these various objectives, this study aims to significantly contribute to the understanding of the dynamics of passively vibrated sweep tools, providing valuable data for future advancements in agricultural tillage technology.

2. Materials & methods

2.1. Laboratory test of the vibration of sweep spring configurations

2.1.1. Laboratory test and DEM model of the passively vibrated sweep tool

The laboratory tests were conducted at the Institute of Technology of the Hungarian University of Agriculture and Life Sciences in Gödöllő, Hungary. During these measurements, an agricultural sweep was employed, with its shank supported by various plate spring configurations (Fig. 1), including 4, 8, 12, 16, 20, 24, 28, and 32 springs. This arrangement was specifically designed to facilitate passive vibration in the sweep. In the initial test, these different spring configurations were investigated using a laboratory ringing test to determine the resulting eigenfrequencies and damping factors of the vibrated sweep tools. The dimensions of the springs, illustrated in Fig. 1 (and also later in Fig. 4), were situated between two supporting surfaces of the instrument, ensuring accurate and controlled testing conditions.

In the initial phase, the system's inherent frequencies and damping were examined applying various spring configurations (as shown in Fig. 1). During the ringing test, a load force of 200 N was applied, and a hammer was used manually to deliver the initial impact to the vibrating system. To enhance the measurement layout, a similar model was improved in DEM simulation (Cundall, 1971; Cundall & Strack, 1979). This approach proved invaluable for investigating the phenomenon observed in the ringing test and in calibrating the DEM model based on the test results.

Yade discrete element simulation software (Smilauer et al., 2015) was employed in this study. The particle-particle and particle-facet connection model used in the DEM simulation was consistent with the methodology applied in the study conducted by Tamás and Bernon (2021). In the DEM simulation, the passively vibrated sweep tool was represented as an STL geometry. However, in the Yade DEM software, this STL geometry was configured as a free body, allowing it to move in the model as discrete particles. It is important to note that simulating the STL geometry as a free body presented several challenges, as the standard harmonic motion engine in the Yade DEM software could only facilitate forced movement in the model. This provided infinitely high energy to the system, similar to the simulation conducted by Keppler et al. (2015). To address this challenge and to simulate the STL body of the sweep as a free body, a multi-step process was implemented. First, the STL triangles (as facets) were clumped together. Subsequently, the mass moment of inertia "tensor" (expressed in kg m^2) were calculated at the output coordinate system. These parameters were obtained from SolidWorks 2021 CAD (Dassault Sistèmes Solid Works Corp., USA) modelling software. The specific inertia tensor parameters of the sweep used in this study were as follows:

$$I_{sweep} = \begin{bmatrix} I_{xx} = 2.6007 & I_{xy} = -0.0192 & I_{xz} = -0.0083 \\ I_{yx} = -0.0192 & I_{yy} = 0.7211 & I_{yz} = 1.0619 \\ I_{zx} = -0.0083 & I_{zy} = 1.0619 & I_{zz} = 1.9056 \end{bmatrix} \tag{1}$$

The values of the diagonal of this matrix shall be specified in the simulation setup. The centre of mass R (m) of the sweep tool was calculated by SolidWorks 2021 CAD software:

$$R_{sweep} = [x = -0.0051 \quad y = 0.4930 \quad z = 0.2709] \tag{2}$$

In the simulation setup, the mass of the simulated sweep tool was defined as 7.692 kg, corresponding to the weight of the actual sweep with the shank. The density of the sweep was calculated to be 10865.5 kg m^{-3}. The volume and surface area of the STL model of the tool were determined to be 0.0007 m^3 and 0.1359 m^2, respectively. The degree of freedom (DoF) of the geometry's translation motion was restricted along the X-axis, while rotational motion was allowed around the X axis. Using these settings, the model of the sweep was able to move in a manner consistent with the actual implement without the need for artificial damping.

In the DEM model of the ringing test, the support springs were simulated using three spherical-shaped particles supported by another sphere. Simultaneously, the centre of the sweep tool's rotations was contained in a specially adapted sphere, located in the hole formed at the end of the shank (refer to Fig. 1). The degrees of freedom of the particles simulated the spring's translational motion, which was allowed in the Y direction, while rotational freedom was permitted around the Y axis. The supporting sphere (Fig. 1c) was fixed in space, and the tool's speed was set. The DoFs of the sphere, used as the load in the calibrations, were allowed along the Y and Z axes.

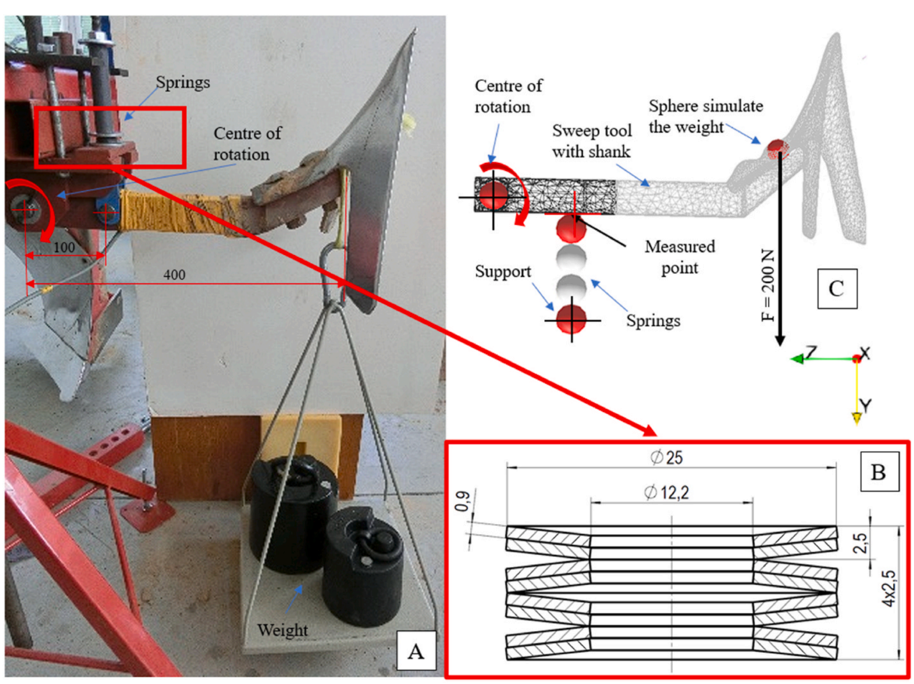

Fig. 1. The a) laboratory ringing test of the passively vibrated sweep tool (with 4 springs), b) DIN 2093 plate spring (4 spring configuration as a unit) with the main dimensions, and the c) DEM model of the passively vibrated sweep tool. (Dimensions are in mm, F-load force [N].)

Although the STL geometry of the sweep tool was treated as one “clumped” body in the simulation, it was split into two halves. This split was necessary because the lower half (grey) measured the draught force without being affected by the spheres simulating the springs, whereas the upper (black) half of the sweep tool’s model was influenced by the forces applied by the spheres. Due to these considerations, the upper and lower halves had to be treated separately in the simulations involving the simulated draught force. During DEM calibration, the micromechanical parameters of the model were used with the values given in Table 1.

In the simulation, a 200 N load force was represented by a sphere with a radius of 15 mm. To match the real test conditions, the density of this sphere was increased to $1.866 \cdot 10^6$ kg m^{-3}, ensuring its weight was similar to the actual test. The sphere’s DoFs simulated the weight, allowing translational movement along the Y and Z axes while locking rotational movements.

During the calibration procedures, local damping was solely influenced by the movement of the spheres simulating the springs in the DEM model. Damping for other geometries in the DEM simulations was set to zero. It is important to note that artificial damping was not considered appropriate for usage, because it does not accurately model the real physical impact of the soil in the DEM model.

In the laboratory ringing test, force fluctuations were measured by a strain gauge attached to the shank and analysed at a frequency of 2400 Hz. In the DEM simulations, the displacement of the tool was recorded at the designated point indicated in Fig. 1c. A spring unit in the current study was built by combining two pieces of trapezoidal springs in parallel (Fig. 1b). The number of springs refers to number of units in the series connected (Fig. 1b). These trapezoidal springs (DIN 2093) worked linearly within the specified range in both the test as well as the simulation. This linear operation allowed the direct comparison and calibration of force vibration and displacement vibration. (Fig. 2).

In fact, the values of frequencies and dampings generated in the measurement and DEM model can be compared. The calculated spring arrangements’ (Figs. 1b and 4c) stiffnesses (DIN 2093) were as follows: 4–$7.5 \cdot 10^5$ N m^{-1}; 8–$3.75 \cdot 10^5$ N m^{-1}; 12–$2.5 \cdot 10^5$ N m^{-1}; 16–$1.87 \cdot 10^5$ N m^{-1}; 20–$1.5 \cdot 10^5$ N m^{-1}; 24–$1.25 \cdot 10^5$ N m^{-1}; 28–$1.07 \cdot 10^5$; 32–$0.94 \cdot 10^5$ N m^{-1}.

Both in the measurement and the simulation, the occurring frequency (f_d) and the damping factor (ζ) were analysed using the following equations:

$$f_d \equiv \frac{1}{T_d}, T_d = \frac{2\pi}{\omega_d} \tag{3}$$

where the logarithmic decrements (Λ) are in both cases:

$$\Lambda_{measured} = \frac{1}{n} ln \frac{A_1}{A_{n+1}}, \Lambda_{simulated} = \frac{1}{n} ln \frac{A_1}{A_{n+1}} \tag{4}$$

Based on Eqn. (4), the damping factor can be calculated both in the measurement and in the simulation with the following equations:

$$\zeta_{measured} = \frac{\Lambda_{measured}}{\sqrt{4\pi^2 + \Lambda^2_{measured}}}, \zeta_{simulated} = \frac{\Lambda_{simulated}}{\sqrt{4\pi^2 + \Lambda^2_{simulated}}} \tag{5}$$

An algorithm was developed in Python to automatically determine the parameters in Eqns. (3)–(5). Consequently, the length of time of a period determines the frequency horizontally, and the lengths of the amplitudes can be calculated vertically (Fig. 3). Using the algorithm introduced earlier in equations (3)–(5), the frequency and damping factor of both the test and the DEM simulation could be compared. In this study, the micromechanical parameters of the DEM calibration model were fine-tuned using a GA based on the frequency and damping factor obtained from the test results, implemented with PyGAD software (Gad, 2021; Meola et al., 2023; Zhu, 2021).

Table 1
The micromechanical parameters utilised in DEM model of the ringing test.

Property of the STL geometry (dynamic)	Value	Source
Young’s modulus [Pa]	$1 \cdot 10^9$	Tamás and Bernon (2021)
Poisson’s ratio [−]	0.3	Tamás and Bernon (2021)
Density [kg·m^{-3}]	10865.5	calculated
Friction angle [°]	40	Tamás and Bernon (2021)
Property of the loading sphere element (dynamic)		
Young’s modulus [Pa]	$1 \cdot 10^7$	selected
Poisson’s ratio [−]	0.3	Tamás and Bernon (2021)
Density [kg·m^{-3}]	$1.866 \cdot 10^6$	calculated to be 20 kg
Friction angle [°]	60	selected
Radius [m]	0.015	selected
Property of the spheres mimicking the spring (dynamic)		
Young’s modulus [Pa]	$1 \cdot 10^6$-$5 \cdot 10^8$	calibrated by PyGAD
Poisson’s ratio [−]	0.3	Tamás and Bernon (2021)
Local damp [−]	0.008–0.03	calibrated by PyGAD
Density [kg·m^{-3}]	100	selected
Friction angle [°]	5	selected
Normal cohesion [Pa]	$2 \cdot 10^4$	selected
Shear cohesion [Pa]	$1 \cdot 10^4$	selected
Eta roll = Eta twist [−]	0.001	selected
Radius [m]	0.02	selected
Ball in the centre of the tool’s rotation which holds and moves the sweep tool’s model (fixed)		
Young’s modulus [Pa]	$1 \cdot 10^9$	selected
Poisson’s ratio [−]	0.3	Tamás and Bernon (2021)
Density [kg·m^{-3}]	7850	selected
Friction angle [°]	5	selected
Radius [m]	0.019	selected
Timestep [s]	$4.969 \cdot 10^{-6}$	calibrated

2.1.2. Soil bin study and DEM model of the passively vibrated sweep tool

The draught force was measured in a soil bin located in the laboratory of the Institute of Technology of the Hungarian University of Agriculture and Life Sciences at a tillage depth of 150 mm. The measurement procedures utilised a low-speed interval of 0.65–0.70 m s^{-1} (Table 2). In each case of the soil bin study, the same sandy soil was used as in the study by Tamás (2018) to ensure reproducibility. The average soil gravimetric moisture content was approximately 3.96% (dry basis), with a cohesion of 6.4 kPa and an internal friction angle of 32.3°.

In the soil bin measurement, a sweep tool with a width of 300 mm and an attack angle of 20° was utilised, maintaining the same geometry as in the study by Tamás and Bernon (2021). The measurement setup is illustrated in Fig. 4a, where the draught force was measured using a strain-gauged shank. Additionally, the displacement of the tool was recorded with a displacement sensor (HBM, W50K, 1177), positioned 100 mm from the centre of the tool’s rotation (Fig. 4a). Fig. 4b displays the arrangement of springs within the sweep tool, and Fig. 4c shows the spring configurations (4, 8, 12, 16, 20, 24, 28, 32 springs) previously calibrated in the laboratory ringing test and employed in the laboratory soil bin test for measurements of the passively vibrated sweep tool. In both simulations, the utilised timesteps were calibrated as described in the study by Tamás (2018). The utilised timestep in the ringing and the soil bin simulations were $4.969 \cdot 10^{-6}$ and $4.354 \cdot 10^{-6}$, respectively.

In the DEM simulations, the same geometrical conditions were applied as in the laboratory soil bin test. However, for practical reasons a supporting spring was used instead of a pulling spring arrangement. The depth of the soil bin in the DEM model was set at 250 mm, the width at 1000 mm, and the length at 1000 mm in the initial attempt and 2000 mm for the final simulations of the interaction between the soil and the

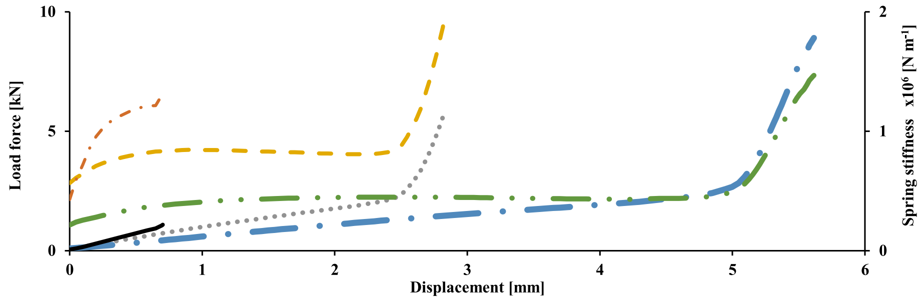

Fig. 2. The results of the spring compression test of DIN 2093 (25x12.2x0.9) single spring (load force –, spring stiffness - ·- ·-), 4-springs (load force ····, spring stiffness – – –) and 8-springs (load force - ·- ·- ·, spring stiffness -·····-) configuration.

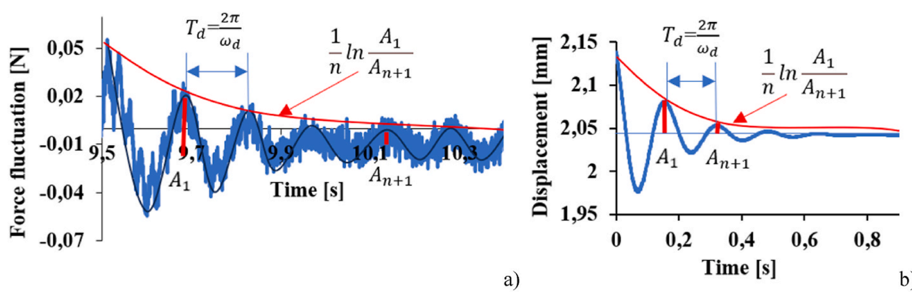

Fig. 3. The a) measurement of the force fluctuation with 200 N load in the laboratory ringing test and the b) DEM displacement-based simulated damped free vibration with simulated 200 N load. (T_d- periodic time (s), ω_d - eigenfrequency (s^{-1}), A – amplitudes (mm) in the logarithmic decrements).

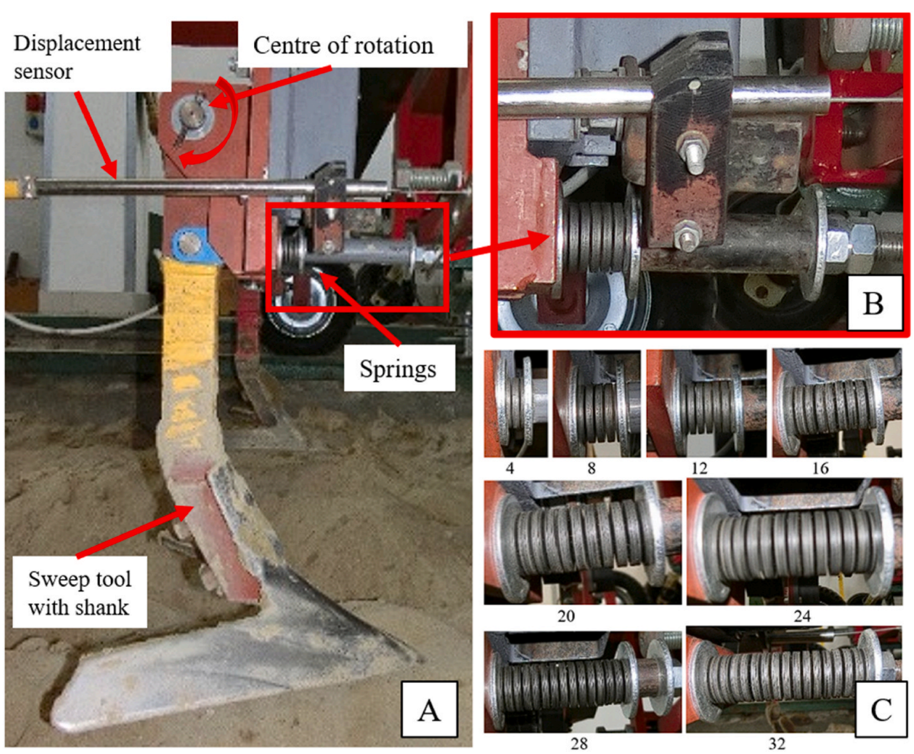

Fig. 4. The layout of the a) laboratory soil bin measurement of the passively vibrated sweep tool, the b) place of the springs, and the c) utilised spring configurations with 4, 8, 12, 16, 20, 24, 28, 32 springs.

passively vibrated sweep. These dimensions were chosen to eliminate walling effects during the simulations.

The DEM studies were conducted on three types of particle assemblies (Fig. 5a), using the same particle shape, geometrical conditions (Fig. 5b) and contact models in the particle-particle and particle-facet connections as had been employed in the study by Tamás and Bernon (2021). This enabled the analysis of different soil textures' behaviour to describe the specific physical phenomenon. The utilised Young's modulus, Poisson's ratio and particle density in all three types of particle assemblies were $1{\cdot}10^7$ Pa, 0.4 and 2700 kg m^{-3}, respectively. As

Table 2
The measurement and the calibration of the DEM model results of the different springs configuration stiffnesses' effected frequency and damping with 200N preload in the ringing test.

Number of springs [−]	Measured eigen-frequency [Hz]	Measured damping [−]	DEM spring Young's modulus [Pa]	DEM damping coefficient [−]	Calibrated eigen-frequency [Hz]	Calibrated damping [−]	Fitness	Relative error [%] frequency	Relative error [%] damping	Offset of the support sphere [mm]
4	9.37499	0.12396	$4.30101 \cdot 10^8$	0.01885	9.43821	0.12296	18304.2	0.00669	0.00815	+3
8	7.00389	0.08929	$2.62542 \cdot 10^8$	0.00996	7.02043	0.08848	46544.9	0.00235	0.00912	+1
12	6.11854	0.04162	$1.91868 \cdot 10^8$	0.00933	5.98601	0.04151	17831.7	0.02213	0.00253	−1
16	6.09137	0.20270	$1.89907 \cdot 10^8$	0.01871	6.14112	0.19256	2344.3	0.00810	0.05264	−3
20	6.02258	0.07071	$1.82521 \cdot 10^8$	0.01663	5.83839	0.07118	4743.8	0.03154	0.00668	−5
24	6.80369	0.27364	$2.47654 \cdot 10^8$	0.02810	6.88610	0.28501	2096.1	0.01196	0.03986	−8
28	5.48195	0.11458	$1.65381 \cdot 10^8$	0.01041	5.38528	0.11465	93484.5	0.01795	0.00059	−8
32	4.78087	0.17708	$1.44069 \cdot 10^8$	0.01653	4.84508	0.17803	14082.1	0.01325	0.00535	−12

Table 3
Draughts of the passively vibrating and the rigid sweep tool at certain speeds. The line indicated a significant decrease in the draught with the 16 springs configuration is highlighted with bold letters. (Std.-standard deviation, vel.-velocity, disp.-displacement, red.-reduction).

Number of. springs [-]	Mean vel. [m s^{-1}]	Std. vel. [m s^{-1}]	Mean. rigid [N]	Std. rigid [N]	Mean vibrating [N]	Std. vibrating [N]	Mean disp. [mm]	Std. disp. [mm]	Red. [%]
4	0.70	0.06	335.57	13.41	319.12	7.86	0.183	0.061	4.90
8	0.68	0.05	332.50	13.70	320.31	7.92	2.096	0.089	3.67
12	0.62	0.05	344.77	13.58	331.74	9.31	3.339	0.061	3.78
16	**0.68**	**0.07**	**341.56**	**13.14**	**317.71**	**8.69**	**4.751**	**0.066**	**6.98**
20	0.57	0.09	331.40	13.56	331.80	8.35	6.220	0.058	−0.12
24	0.59	0.04	343.52	14.83	331.15	9.10	7.773	0.131	3.60
28	0.62	0.05	341.33	13.99	347.45	10.23	8.380	0.185	−1.79
32	0.52	0.04	335.81	14.54	354.35	9.42	12.487	0.131	−5.52

depicted in Fig. 5a, assembly (A) consisted of spheres, while assembly (B) included clumps, and assembly (C) contained elongated clumps, all having the same shape, geometric parameters, and distributions as those studied in the research by Tamás and Bernon (2021). The utilised particles' geometries were taken into consideration in other studies, where the effect of the particle shape (Ono et al., 2013) or aggregate was significant (Foldager et al., 2022; Barbosa et al., 2022) in the simulation of the soil's rheological nature.

In the DEM simulations of the soil bin study, one of the main parameters investigated was the kinetic energy of the entire system, calculated automatically using Yade's embedded method (Šmilauer et al., 2015; Šmilauer & Chareyre, 2010). Subsequently, the kinetic energy of the sweep tool model and the kinetic energy of the particle assembly were separately evaluated, considering both the translational and rotational movements. The total kinetic energy (E_k) of all individual bodies separately as spheres or clumps and facets or as a whole in the simulation was calculated by adding translational and rotational kinetic energies, using the following equation:

$$E_k = \frac{1}{2}\sum_{b=0}^{N_b-1}\left(m_b v_b^2 + I_b {\omega_b}^2\right) \tag{6}$$

where m_b is mass [kg], v_b is translational velocity [m s^{-1}], I_b is the mass moment of inertia [kg m^2], and ω_b means the angular velocity [rad s^{-1}] of the single body (indicated with subscript b) and N_b means the number of the bodies in the DEM simulation.

2.2. Genetic algorithm (GA) utilised in the calibration procedure

A relatively recent approach in this field, a GA, was employed for the calibration of parameters in the DEM model of the soil and the passively vibrating sweep tool. Using this algorithm, the DEM calibration model of the vibrated sweep tool and the micromechanical parameters of the particle assemblies used were separately calibrated, relying on the results from the laboratory tests. These simulations were conducted using PYGAD software (Gad, 2021; Meola et al., 2023; Zhu, 2021), which was integrated with both the ringing and simulations of the soil and the passively vibrated sweep in the Yade DEM software.

2.2.1. Utilising a genetic algorithm (GA) in the calibrations of sweep spring configurations

In the DEM model of the ringing test, the oscillation of the sweep and shank, facilitated by different springs, was calibrated using a GA. These calibrations were based on the frequencies and damping values obtained from the laboratory ringing test. The frequencies and damping factors were previously measured and assessed by means of a Python code algorithm. The calibration was achieved with the help of PYGAD GA software (Gad, 2021). During these calibrations, specific target values for the frequency and damping factor were predetermined. The existing DEM model of the ringing test was employed for calibration purposes (refer to Table 2). The same algorithm was applied to analyse the resulting frequency and damping factor in the DEM simulation, and the results were integrated using the following fitness function:

$$fitness = \frac{1}{RE_{freq} \bullet RE_{damp}} \tag{7}$$

where,

$$RE_{freq} = \left|\frac{freq_{sim} - freq_{target}}{freq_{target}}\right| \tag{8}$$

and

$$RE_{damp} = \left|\frac{damp_{sim} - damp_{target}}{damp_{target}}\right| \tag{9}$$

In the PYGAD genetic algorithm, 5 generations, 20 populations, 7 parents, 0.01% gene mutation rate, and 2 genes (representing DEM parameters) were specified. During these calibration simulations, the micromechanical Young's modulus and the local damping were considered as the variables, corresponding to the 2 genes. These parameters defined the characteristics of the particles simulating the

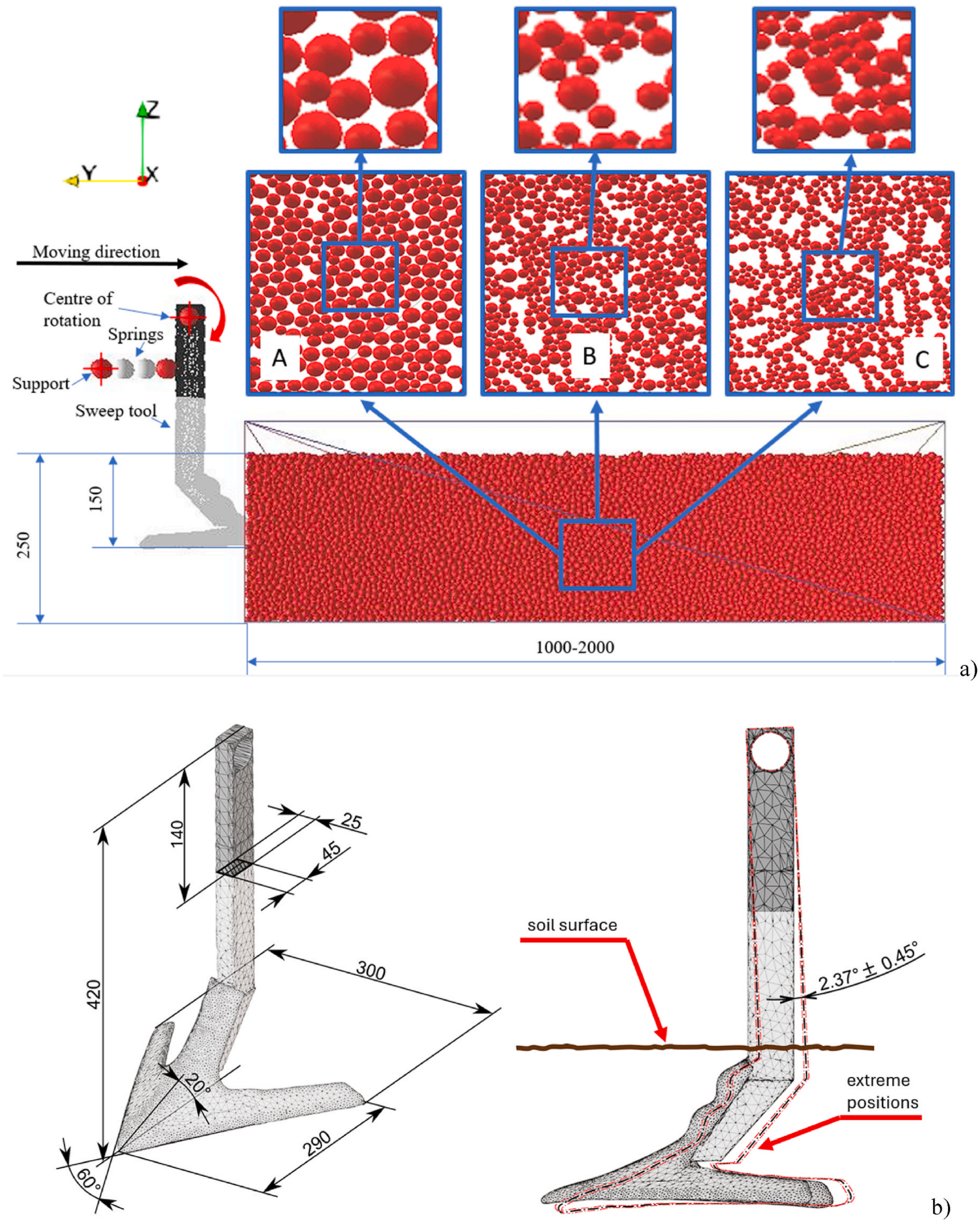

Fig. 5. The a) DEM model which was utilised with three different particle assemblies, (A)-Spheres, (B)-Clump, (C)-Clump elongated. 3D scanned b) sweep geometry (left) with dimensions, and the passively vibrating (right) 16 spring sweep configuration. (extreme positions – - – -, soil surface ~~~~~~) (Dimensions are in mm.).

mechanical properties of real springs. These parameters were defined within specific intervals as gene spaces, with the micromechanical Young's modulus ranging from $1{\cdot}10^6$ Pa to $5{\cdot}10^8$ Pa and the local damping ranging from 0.008 to 0.03. It is important to note that damping for all other DEM components was disabled during the simulation process. Using this method, 85 simulations were conducted, each taking approximately 1 h to complete.

The calibration results are presented in Table 2, where a parameter set was chosen based on the lowest relative error and the highest fitness value. During calibration, the eigenfrequencies that had been measured previously were set based on the stiffness and local damping of the particles, modelling the actual (real-world) spring configurations. This calibration process resulted in a single appropriate parameter set.

2.2.2. *A genetic algorithm utilised in the draught calibration*

During the draught calibrations, a rigid sweep tool with fixed DoF was employed in the DEM (Chen et al., 2013; Tekeste et al., 2019; Ucgul et al., 2014). The precise draught measurement data obtained from the laboratory soil bin study were used as the calibration target. In this calibration process, the following fitness function was utilised:

$$\text{fitness} = \frac{1}{RE_{Draught}} \tag{10}$$

where the relative error (RE) was calculated as follows:

$$RE_{Draught} = \left| \frac{Draught_{sim} - Draught_{target}}{Draught_{target}} \right| \tag{11}$$

In the soil DEM model calibration, a rigid tool (with no inertia) was moved through the particle assembly at the same speed as in the actual laboratory soil bin test. During this calibration, the mean value of the measured draught force was set as the target value for calibration.

In the PYGAD genetic algorithm, similarly to the calibration of the ringing test, the following parameters were set: 5 generations, 20 populations, 7 parents, 0.01 percent mutation rate, and 3 genes representing DEM micromechanical parameters. In these calibration simulations, particle-particle and particle-facet contact parameters were explored, such as the micromechanical friction angle, micromechanical normal cohesion, and rolling/twisting friction coefficients (Ai et al., 2011; Holmes et al., 2016; Wensrich & Katterfeld, 2012). These parameters were defined within specific intervals, where the lowest and highest values were set. The intervals for the parameters were as follows: 5°–50° for the micromechanical friction angle, $1{\bullet}10^1$-$5{\bullet}10^4$ Pa for micromechanical normal cohesion (normal cohesion = 2•shear cohesion), and 0.001–0.9 for the rolling and twisting (rolling coefficient = twisting coefficient) friction coefficient (Horváth et al., 2019). The mean draught force in the DEM model was calculated after 0.5 m of sweep tool displacement, which was considered to be the steady state region. The "artificial" local damping was disabled in these simulations, as it was in the research by Tamás (2018).

During this calibration procedure, 85 simulations were executed, taking nearly 4 h per simulation. The draught force calibration for the soil-sweep interaction with a rigid shank yielded multiple parameter sets, where the draught force was calibrated with less than 10% relative error (Tables 4–6).

2.3. Direct shear box test for laboratory and DEM parameter set evaluation generated by the GA

In line with previous studies by Tamás and Bernon (2021), the direct shear box test emerged as the most reliable method for analysing the mechanical properties of a particle assembly in DEM simulations (Sadek et al., 2011; Ucgul et al., 2015). As in the methodology employed by Tamás and Bernon (2021), various soil samples with different moisture contents were prepared and tested using the laboratory direct shear box test. This approach aimed to establish the relationship between soil shear strength, internal friction angle, and the gravimetric moisture content of the sandy soil used in the laboratory soil bin (Tamás, 2018). Specifically, soil samples with dry basis moisture contents of 0.19%, 3.96%, 10.17%, and 17.62% were tested. The corresponding measured cohesions and internal friction angles were 8.7 kPa and 30°, 6.4 kPa and 32.3°, 9.8 kPa and 33.28°, and 5.2 kPa and 34.86°, respectively.

As the GA yielded several suitable parameter combinations for accurately simulating the draught force in the different particle assemblies, the parameter set or particle assembly demonstrating the best match between its direct shear box test results and the real measurements was selected for the final DEM model of the soil's interaction with the passively vibrated sweep tool. The same direct shear box simulation procedure as used in the study by Tamás and Bernon (2021) was employed for this purpose. The objective was to exclude micromechanical parameter sets calibrated from the draught force that did not accurately simulate the mechanical characteristics of the real sandy soil at the appropriate scale. Consequently, following the tests using the DEM model of the direct shear box test, only one parameter set was accepted for assembly (A), (B), and (C).

2.4. Fast Fourier Transform (FFT) method for frequency analyses

In this study, the FFT method was employed to analyse the frequency range resulting from the draught force and the displacement of the shank's control point as functions of time. Fourier analysis is a technique used to convert a signal from its original domain into a representation in the frequency domain, providing insights into the most active frequencies along with their amplitudes during the tillage process (Upadhyaya et al., 1987). The FFT results from the laboratory soil bin test and the discrete element simulation were compared. In the DEM simulation, it was possible to analyse the physical phenomena in detail, elucidating the causes behind the reduction in draught force during the tillage process.

A Python code was developed for conducting the FFT analyses. The data measured and simulated in the steady-state region were analysed using FFT. The software considered integer multiples of the primary frequencies in the final results. Prior to the analyses, harmonic signals below 100 Hz were filtered out using a Butterworth low-pass filter. This filtering step ensured that the software could focus on examining the intensity of frequencies (Fenyvesi et al., 2002) resulting from the displacement of the sweep tool and the resulting draught force.

3. Results

3.1. The results of the passively vibrated sweep springs calibrations

The results of the GA calibration are presented in Fig. 6, where each subfigure displays the periodic change of force on the left side (lab. test) and the periodic change of displacement as a function of time on the right side (DEM test), with a 200 N loading force applied. These results are promising as they indicate visually strong matches achieved through the calibration process. By observing the shapes of the curves, it is evident which spring configurations have higher or lower damping characteristics. It should be noted that the comparisons of force-time (laboratory test) and displacement-time (DEM test) diagrams were possible in the calibration procedure because the utilised trapezoidal spring configurations operated with linear spring characteristics in the applied ranges. This enabled comparing the change in force and displacement over time.

The measured and calibrated frequencies are presented in Table 2, with the fitness function and relative error indicating the accuracy of the results. It can be seen in Table 2 that the calibration with GA reduces the RE to a level below 0.06%. The calibrated DEM normal spring stiffness and damping were applied in subsequent soil bin simulations to

Table 4
The results of soil-sweep calibration with the GA for spheres (A) at a speed of 0.62 m s^{-1}. The line indicated by bold letters is the closest to the measured values with the laboratory direct shear box test.

	Friction angle [°]	Normal Cohesion [Pa]	Shear Cohesion [Pa]	EtaRoll = EtaTwist [−]	RE [%]	*Internal friction angle [°]*	*Cohesion [kPa]*
(1)	***13.21312***	***42205.48***	***21102.74***	***0.1052903***	***0.71***	***29.18***	***7.018***
(2)	49.05912	5737.44	2868.72	0.0600936	4.39	39.62	21.891
(3)	13.00226	32510.28	16255.14	0.4456579	0.45	35.58	3.662
(4)	13.04606	49692.50	24846.25	0.0600936	6.62	35.77	4.208

Table 5
The results of soil-sweep calibration with the GA for clumps (B) at a speed of 0.62 m s^{-1}. The line indicated by bold letters is the closest to the measured values with the laboratory direct shear box test.

	Friction angle [°]	*Normal Cohesion [Pa]*	*Shear Cohesion [Pa]*	*EtaRoll = EtaTwist [−]*	*RE [%]*	*Internal friction angle [°]*	*Cohesion [kPa]*
(5)	11.0151	32295.48	16147.74	0.0070	2.19	34.71	18.51
(6)	11.7720	38002.63	19001.31	0.0077	4.75	30.04	16.78
(7)	11.7720	18434.15	9217.08	0.0248	1.61	32.44	22.04
(8)	9.2435	10035.10	5017.55	0.0646	4.38	36.16	11.41
(9)	***12.2174***	***21571.34***	***10785.67***	***0.0107***	***0.20***	***34.64***	***12.95***
(10)	12.2174	10758.43	5379.21	0.0107	1.24	31.84	16.24

Table 6
The results of soil-sweep calibration with the GA for elongated clumps (C) at a speed of 0.62 m s^{-1}. The line indicated by bold letters is the closest to the measured values with the laboratory direct shear box test.

	Friction angle [°]	Normal Cohesion [Pa]	Shear Cohesion [Pa]	EtaRoll = EtaTwist [−]	RE [%]	*Internal friction angle [°]*	*Cohesion [kPa]*
(11)	***6.3017***	***22464.06***	***11232.03***	***0.0632***	***0.99***	**31.34**	**6.44**
(12)	7.5309	35567.77	17783.89	0.0111	1.28	34.18	16.30
(13)	5.8513	20847.37	10423.68	0.0845	1.87	22.09	20.09
(14)	5.8513	14678.12	7339.06	0.0951	2.40	26.92	18.93
(15)	5.0567	35567.77	17783.89	0.0951	3.32	27.26	17.62

establish parameter settings for various sweep tool spring configurations.

To create a fully accurate model, the rotation of the tool was considered in the final simulations. This rotation was controlled by adjusting the offset of the support sphere and was based on the rotational movement of the tool's shank at the measured point (see Fig. 1c), as depicted in the subfigures of Fig. 7. It is important to note that the initial comparisons between the different particle assemblies were conducted solely based on the calibrated spring characteristics.

3.2. The results of the soil bin test

3.2.1. Results of the draught force

The draught force of both the passively vibrating and the rigid sweep tool were measured one pass at a time. Simultaneously, the rotational displacements of the passively vibrating tool were recorded using the displacement sensor. The results of the tool's displacement clearly indicated that the more springs were used, the more the spring system was able to compress, causing the tool to bend backward. However, it is important to note that if this backward bending exceeded a specific threshold, the tool's draught force was greater due to the increased inclination and attack angle of the sweep tool.

Based on the draught force results, it was evident that lower draught forces were obtained with spring settings 4–16 (Fig. 7a, b, c, and d) and 24 (Fig. 7f). A noticeable decrease in draught force was observed with tighter spring settings. Specifically, when 16 springs were used, there was a more significant decrease in the draught force. This indicated that the passively vibrated sweep tool with 16 springs vibrated at the eigenfrequency and amplitude under the given conditions.

3.2.2. Results of FFT of the draught and displacement in laboratory soil bin test

In the FFT results, it was evident that the tool frequencies were lower than 30 Hz for both the stiffest and softest spring settings (Fig. 8). Additionally, in all comparisons based on the draught force, lower frequencies were observed in the passively vibrating sweep tool compared to the FFT of the rigid tool. This difference in frequency could explain the lower draught force, as the relaxation process became more damped. Interpreting this phenomenon from a real physical perspective, the passively vibrating sweep tool probably influenced the development of cracks in the soil during loosening in a similar manner to that observed in the study by Karmar et al., (2005).This effect may have resulted in lower mass transport in the interaction between the soil and the passively vibrated sweep, contributing to the observed reduction in draught force.

Analysing the FFT results of the displacement, they aligned with the findings from the draught FFT results (Fig. 9). However, it is notable that in areas where a reduction in draught force was observed, there was a more pronounced increase in the frequency ratio, particularly concerning the amplitude in the frequency range below 10 Hz. This observation further supported the connection between reduced draught force and specific frequency-amplitude relationships in the interaction of the passively vibrated sweep tool.

The results of the laboratory soil bin study are presented in Table 3. It was evident that the most significant decrease in draught force occurred when the shank of the sweep tool bends backwards. This reduction in draught force can be attributed to the eigenfrequency of the sweep tool, indicating that specific tool configurations, particularly those leading to lower eigenfrequencies, resulted in reduced resistance during the tillage process. This phenomenon was partially due to the vibration of the tool back and forth at a given frequency, hence it was not in constant contact with the soil. Therefore, the power required to overcome friction was also reduced. The changes of the sweep tool's projection surface in the direction of motion can contribute to the phenomenon, where due to the change in the effect of soil failure, the energy required for lower mass transport was also lower. However, both previously mentioned factors, or even their combined presence, can result in the reduction of draught.

3.3. The evaluation of GA calibrations with direct shear box simulations

The calibration of the soil model was carried out solely by utilising the DEM simulation of the soil, based on measurements. Several parameter combinations were identified that met the acceptable relative error criteria (<10%) the results of which were in line with the research results of Roessler et al. (2019). The calibrated combinations were further scrutinised using direct shear box simulations.

Table 4 presents the parameter combinations suitable for the draught calibration of the soil bin, involving assembly (A), made of spherical particles. Table 5 contains combinations for assembly (B), made of clumps, and Table 6 contains combinations for assembly (C), consisting of elongated clumps. These parameter sets were considered appropriate (RE<10%) for the soil bin's draught calibration and were evaluated

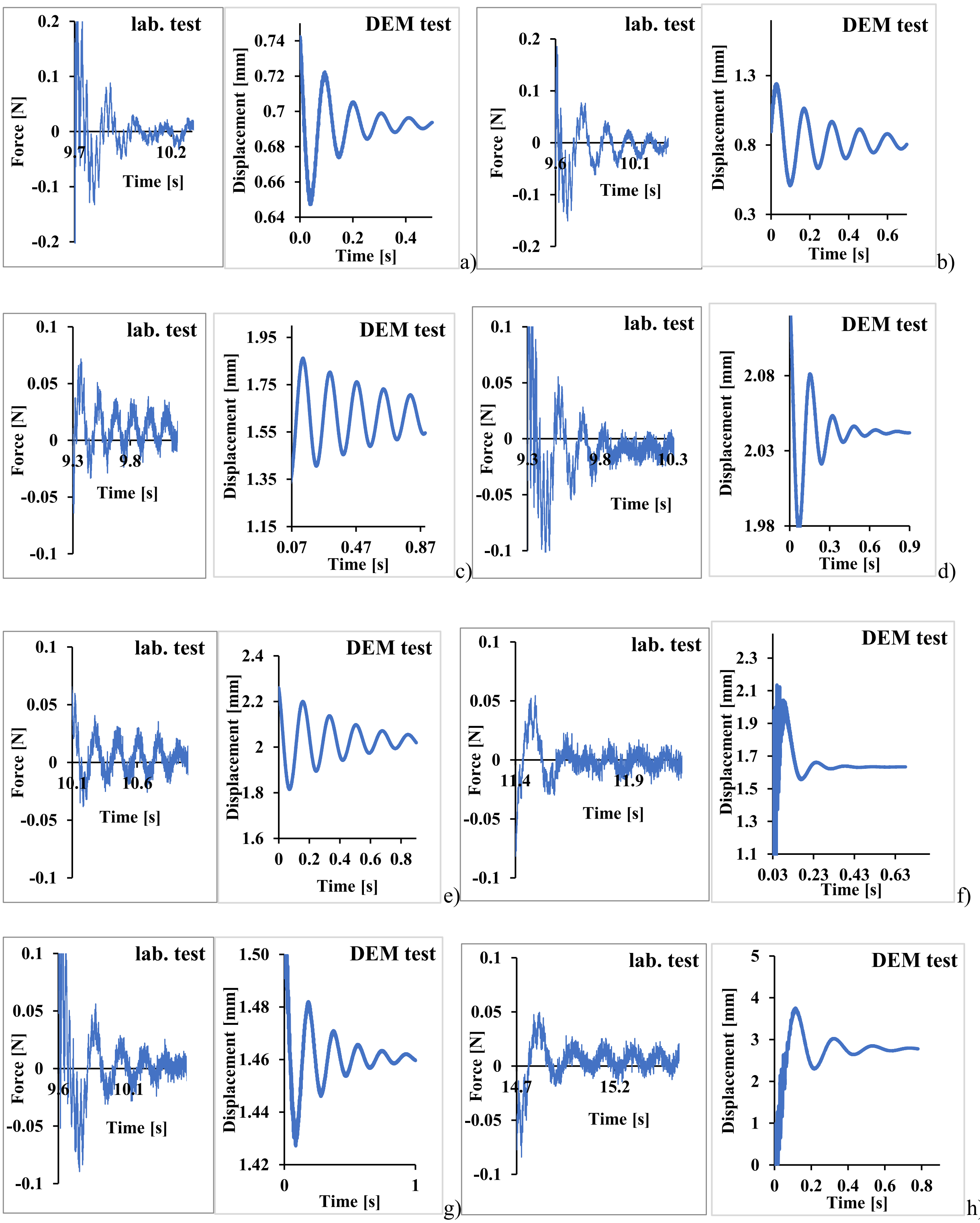

Fig. 6. The vibrations of the sweep's ringing test applications with different spring stiffness properties: a) 4, b) 8, c) 12, d) 16, e) 20, f) 24, g) 28, h) 32. All subfigures on the left side (lab. test) show the result of the laboratory ringing test based on force fluctuation, and the right side (DEM test) shows the calibrated in DEM by PyGAD, while 200N load was applied.

alongside the results of the direct shear box simulations. The resulting internal friction angles and cohesion values were found to be comparable to the outcomes of the laboratory direct shear box test conducted on the actual sandy soil used in the laboratory soil bin test.

In the laboratory soil bin study, the moisture content was 3.96% (dry basis), and the cohesion and the internal friction angle were 6.4 kPa and 32.3°, respectively. All of the calibrated parameter sets were analysed in the DEM simulation of the direct shear box test. Fig. 10 shows the results where the minimum deviation between the individual failure lines is visible, affecting the emerging cohesion and internal friction angle of each calibration result from the GA.

In all three tested assemblies consisting of distinct particle

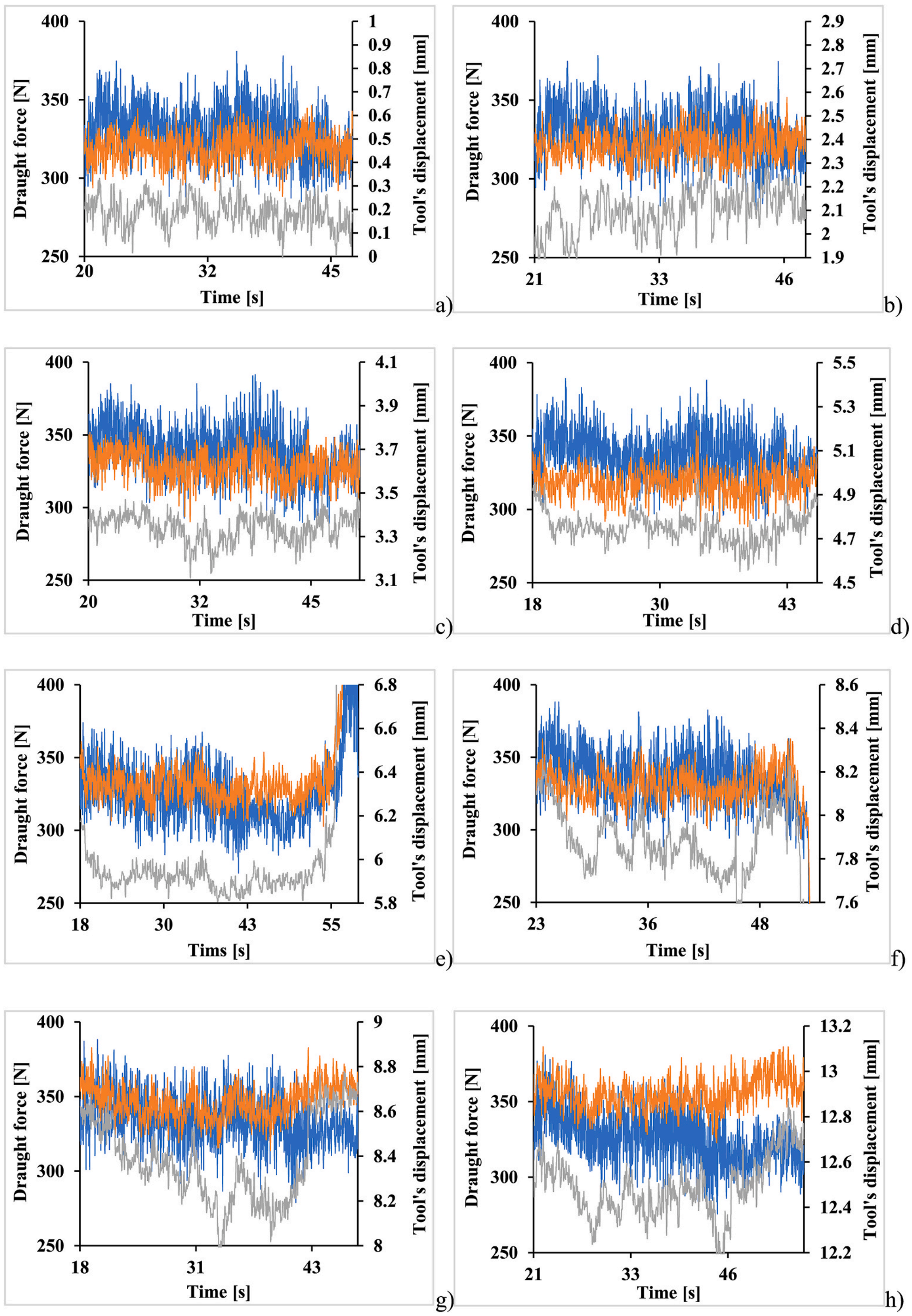

Fig. 7. The laboratory soil bin test results with a) 4, b) 8, c) 12, d) 16, e) 20, f) 24, g) 28, h) 32 springs (— draught of the rigid tool; — draught of the passively vibrated sweep tool; — rotational displacement of the passively vibrated sweep tool).

geometries, it can be recognised that low REs can be obtained with different parameter sets in the draught calibration of the soil-rigid sweep interaction. In this calibration, apart from draught and direct shear box test simulations, the particle assemblies were not tested qualitatively; however, the micromechanical properties of assembly (C) were the closest to the laboratory direct shear box test results.

3.4. Results of DEM model of the passively vibrated sweep's interaction with the soil in three different particle assemblies

The simulated draught forces with the standard deviations are shown in Fig. 11, where the magnitude of the resulting draught forces varied in different ways for each set of springs depending on the spring stiffness. It was evident that the most significant reduction in draught force occurred in assembly (C), consistent with the results of the laboratory soil bin test. Furthermore, in Fig. 11d, e, and f notable differences can be observed in the draught force of the rigid and the passively vibrated sweep tools when 16 springs and 32 springs were selected as the sweep configurations. Significant variations in the fluctuating draught forces were noticeable in each particle assembly. It is worth mentioning that a slightly different development of the draught force was observed in assembly (C), which resulted from the geometry and texture of the particle

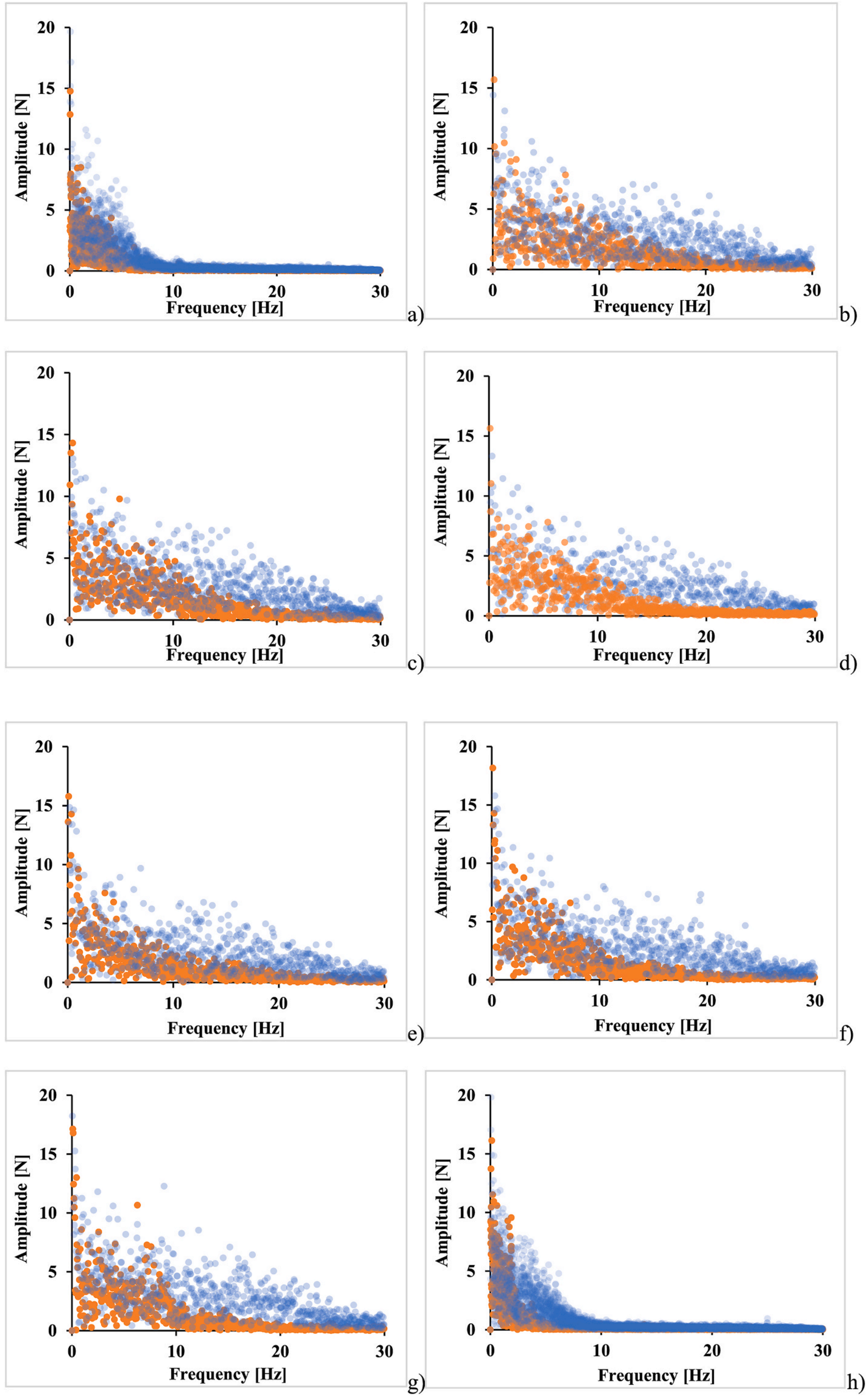

Fig. 8. The results of the FFT of laboratory soil bin test with different spring configurations of the • rigid tool and the • passively vibrated sweep tool, where a) 4, b) 8, c) 12, d) 16, e) 20, f) 24, g) 28, h) 32 springs.

assembly.

The draught force depending on the spring stiffness is summarised in Table 7, where, in addition to the draught force values, the percentage of draught reductions compared to the draught force of the rigid sweep tool are presented. While the decrease in the draught force can also be observed for the spheres in assembly (A), assembly (C) was the most comparable to the laboratory soil bin measurement. From the above results, it can be concluded that in the DEM calibration, when modelling the interaction between the soil and the passively vibrated sweep tool, in addition to calibrating the micromechanical parameter settings of the contact model, it was also necessary to calibrate the geometry of the particles specified in the applied assemblies. This calibration should align with the real physical functioning of the phenomenon being analysed, emphasising the accurate description of the soil texture in the DEM model.

Table 7 shows the draught force reduction in the 2 m long improved version of the DEM model for the interaction between the soil and the passively vibrated sweep. The initial draught force of the rigid sweep

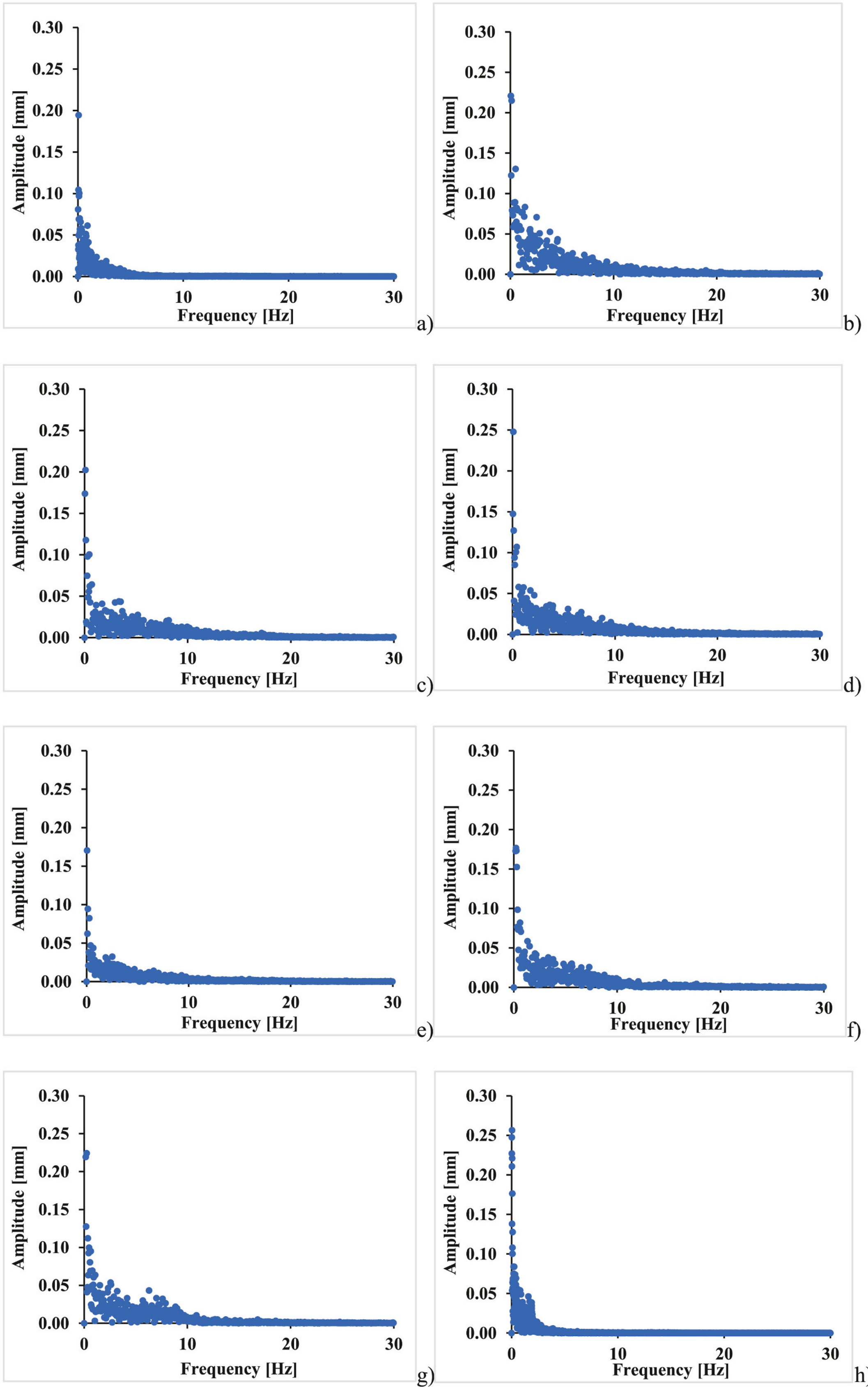

Fig. 9. The results of the FFT on the signal of the sweep tool's displacement (produced by the sweep tool's shaking mechanism) on different spring configurations, where a) 4, b) 8, c) 12, d) 16, e) 20, f) 24, g) 28, h) 32 springs.

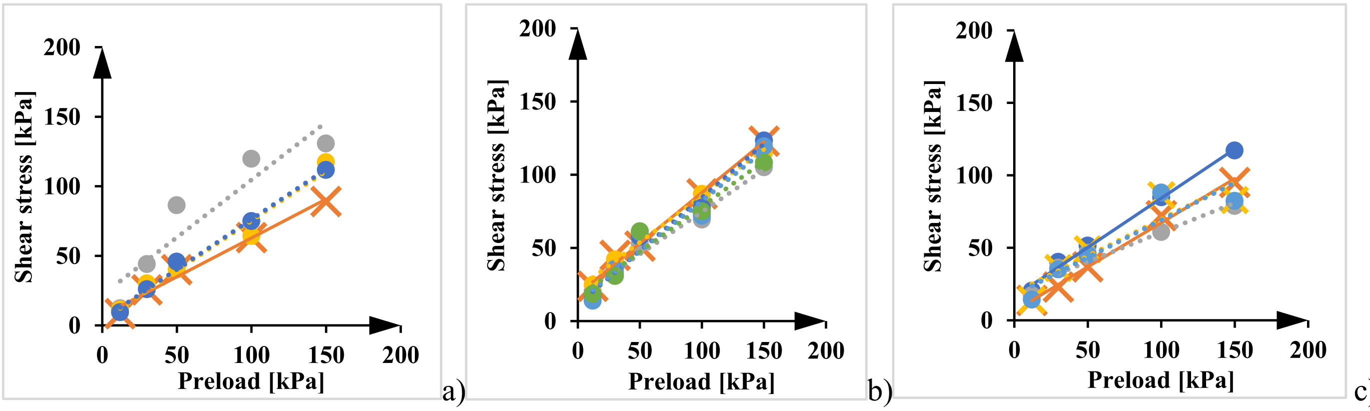

Fig. 10. The results of the direct shear box simulations, a) assembly (A) spheres (-*(1)* R^2*=0.98;* -*(2)* R^2*=0.86;* -*(3)* R^2*=0.97;* -*(4)* R^2*=0.99*), b) assembly (B) clump (-(5) R^2=0.99; -(6) R^2=0.98; -(7) R^2=0.99; -(8) R^2=0.98; -(9) R^2=0.95; -(10) R^2=0.95), c) assembly (C) elongated clump (-(11) R^2=0.99; -*(12)* R^2*=0.99;* -*(13)* R^2*=0.95;* -(14) R^2=0.85; -*(15)* R^2*=0.85)*. (The numbering of markings is consistent with Table 4, 5, and 6.).

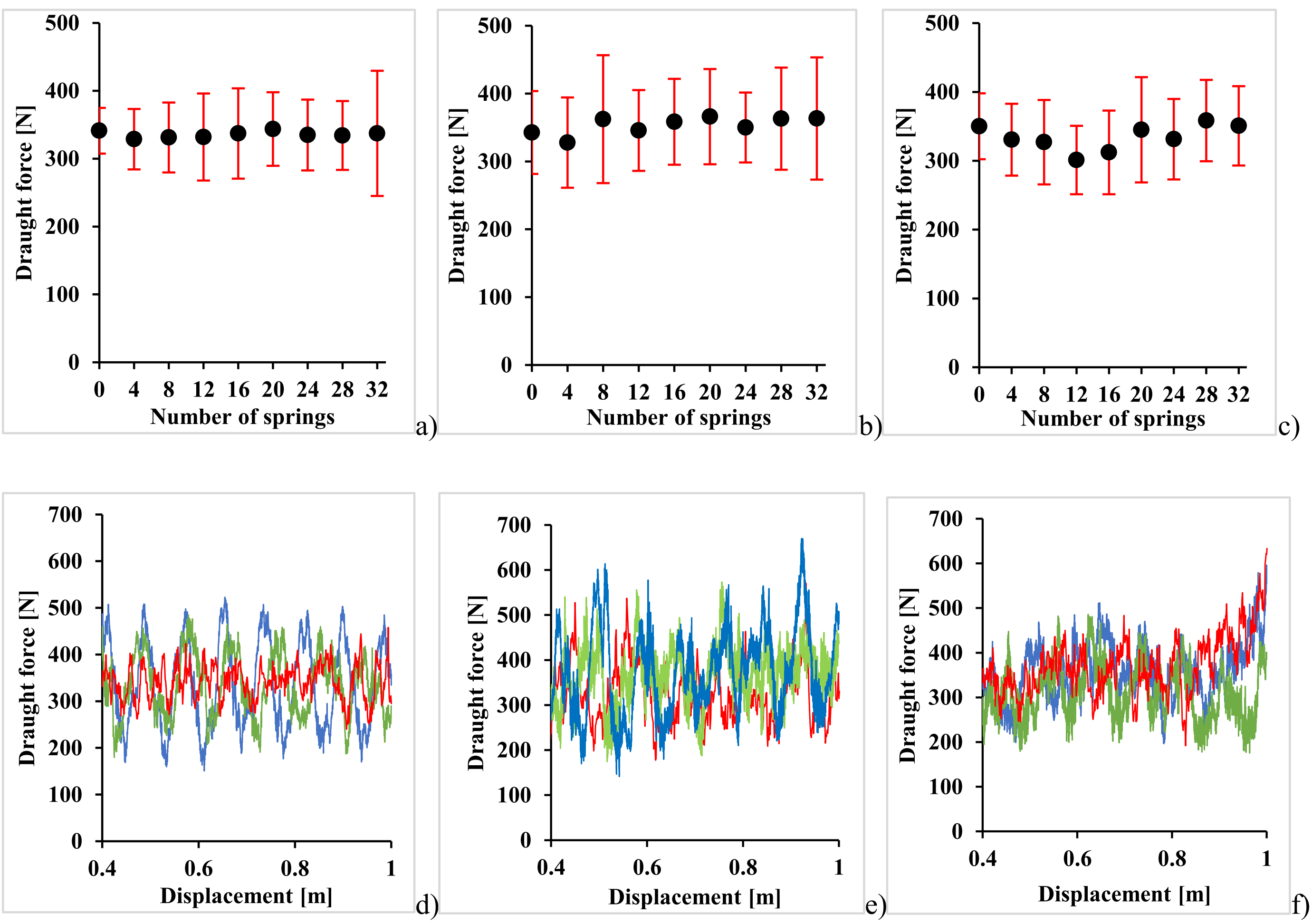

Fig. 11. The mean draught force with the standard deviations of a) assembly (A), b) assembly (B), and c) assembly (C). The resulting draught forces on d) assembly (A), e) assembly (B), and f) assembly (C). (rigid tool, passively vibrated sweep tool with 16 springs, passively vibrated sweep tool with 32 springs).

tool was lower than the previously reported results due to the doubling of the soil DEM model's length in the laboratory soil bin test. This modification allowed for a more accurate representation of the real world conditions and resulted in improved simulation outcomes.

In the simulations, the kinetic energy exhibited specific patterns based on the number of springs used in the sweep tool configurations. The assemblies with the rigid sweep tool had the lowest kinetic energy, indicating minimal vibrational movement. Following this, assemblies with 32 springs showed low kinetic energy, suggesting limited vibration.

In contrast, the assemblies with 4, 8, and 12 springs exhibited decreasing kinetic energy levels. However, when 16 springs were applied there was a notable increase in both the magnitude of kinetic

Table 7
Draughts in DEM of the passively vibrated and the rigid sweep tool at certain speeds. (vel.-velocity, red.-reduction) The column indicated by bold letters is the result of the final (improved) version of the soil-passively vibrated sweep interaction.

Number of. springs	Mean. vel. [m s^{-1}]	Mean. (A) [N]	Red. [%]	Mean (B) [N]	Red. [%]	Mean (C) [N]	Red. [%]	Mean. (C) final [N]	Red. [%]
0 (rigid)	0.68	341.19	–	342.62	–	350.11	–	**311.86**	–
4	0.70	328.72	5.57	327.74	4.35	330.63	5.56	**289.21**	7.26
8	0.68	334.25	2.03	362.32	−5.74	326.99	6.60	**300.13**	3.76
12	0.62	331.95	2.71	345.63	−0.87	301.06	14.01	**300.59**	3.61
16	0.68	337.13	1.19	358.43	−4.61	312.15	10.84	**283.59**	***9.06***
20	0.57	343.73	−0.74	365.98	−6.81	345.02	1.45	**296.99**	4.77
24	0.59	334.89	1.85	350.00	−2.15	331.33	5.36	**309.27**	0.83
28	0.62	334.21	2.05	363.03	−5.95	358.41	−2.37	**305.99**	1.88
32	0.52	337.33	1.13	363.27	−6.02	350.75	−0.18	**301.09**	3.45

energy and its standard deviation across all assemblies. This increase in kinetic energy with 16 springs suggested more vigorous vibrational movement. It is important to highlight that the settings with 16 and 24 springs exhibited the highest damping values, indicating increased resistance to vibrational motion. This damping effect was crucial because, along with appropriate eigenfrequency settings, it significantly influenced the system's kinetic energy. Higher damping values restricted the tool's vibration, resulting in shorter vibrational paths and potentially increased energy transfer to the soil.

The fluctuations in kinetic energy along the simulated length were analysed for different sweep tool configurations (rigid, 16 springs, and 32 springs) in assemblies (A), (B), and (C). The results, depicted in Fig. 12d, e, and f, revealed distinct patterns in kinetic energy fluctuation. For the rigid tool, the kinetic energy exhibited minor fluctuations, indicating stable vibrational behaviour. However, with the DEM models using 16 and 32 springs, there were significant fluctuations with larger amplitudes. Among these configurations, the 32 springs in assembly (A) showed more substantial fluctuations, suggesting intense vibrational activity. Interestingly, assembly (C) with 16 springs displayed the most significant fluctuation in kinetic energy.

This phenomenon was influenced by the texture of the DEM soil model, particularly the geometry of clumps used in the particle assembly. The irregularities in particle shapes and their arrangement contributed to varied vibrational behaviour, leading to the observed fluctuations in kinetic energy.

The deflection of the sweep tool increased as lower spring stiffness

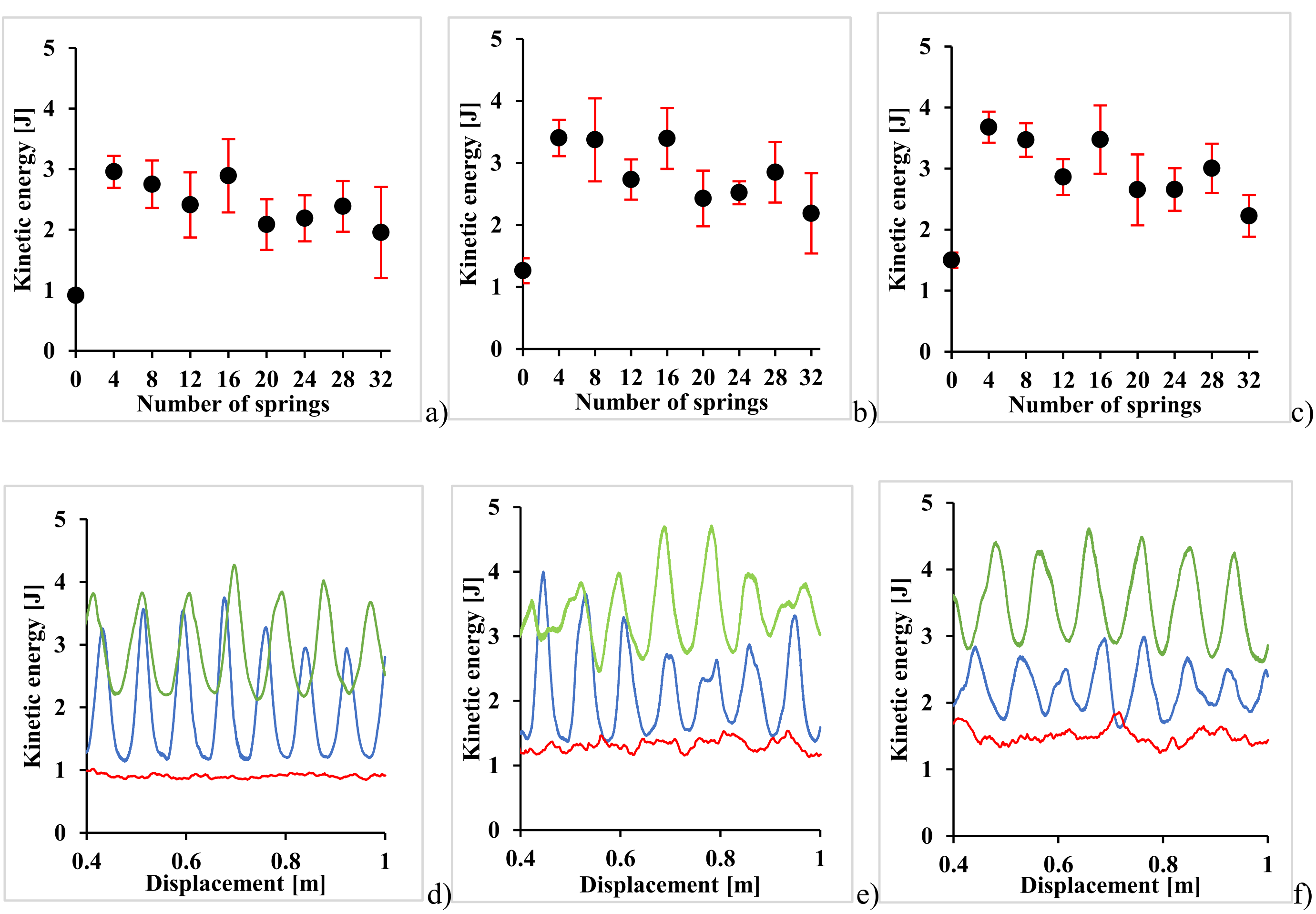

Fig. 12. The mean kinetic energy of the entire DEM model ● with the standard deviations ▬ of a) assembly (A), b) assembly (B) and c) assembly (C). The resulting kinetic energies vs. displacement of the entire DEM modell on d) assembly (A), e) assembly (B), and f) assembly (C). (▬ rigid tool, ▬ passively vibrated sweep tool with 16 springs, ▬ passively vibrated sweep tool with 32 springs).

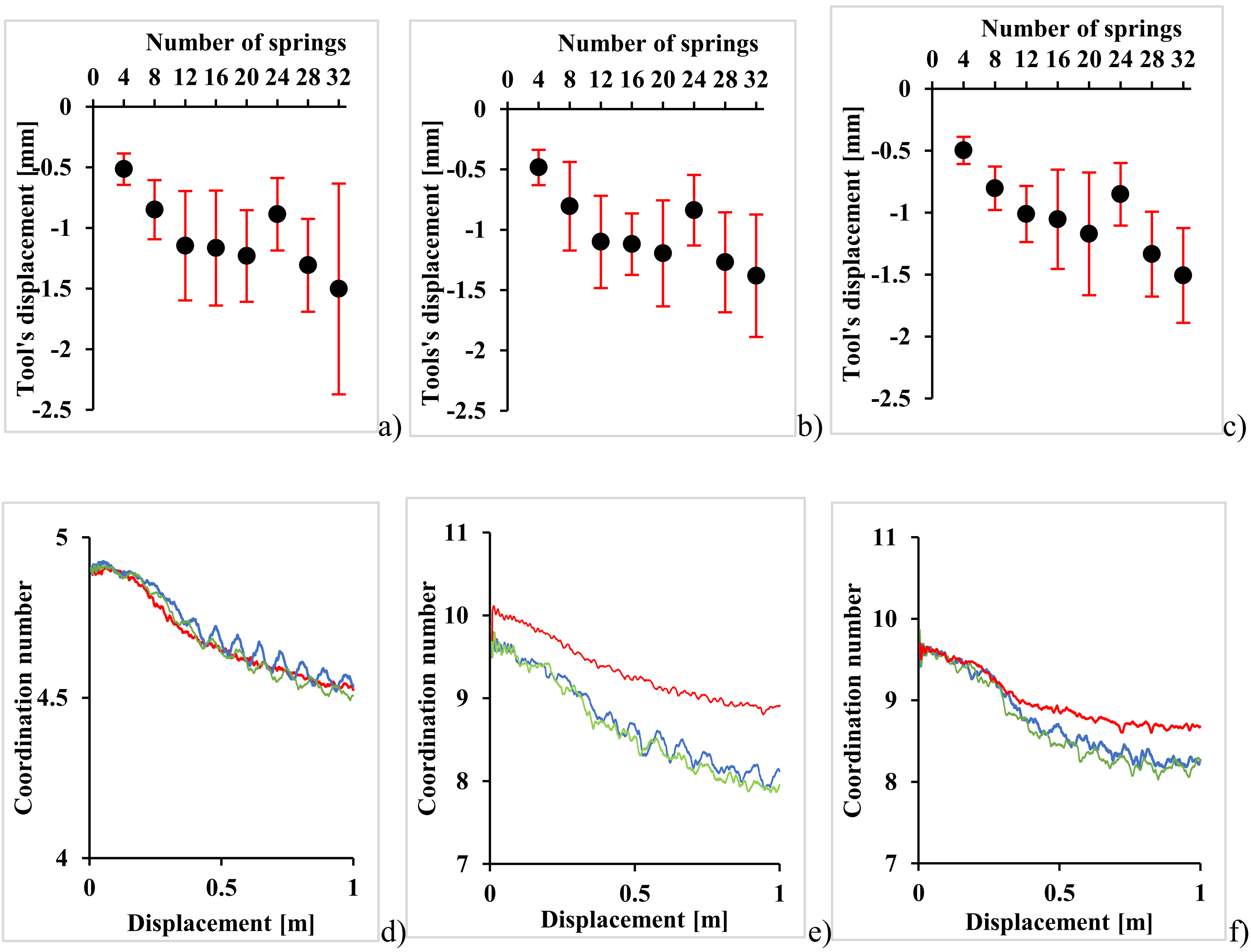

Fig. 13. The ● mean displacement of the tool in the DEM model and the — standard deviations of a) assembly (A), b) assembly (B), and c) assembly (C). The emerging coordination number of d) assembly (A), e) assembly (B), and f) assembly (C). (— rigid tool, — passively vibrated sweep tool with 16 springs, — passively vibrated sweep tool with 32 springs).

was applied, ranging from 4 to 32 springs, as depicted in Fig. 13a, b, and c. Interestingly, when 24 springs were used, the deflection of the tool noticeably decreased. This reduction was attributed to the specific amount of damping applied to this spring configuration at a speed of 0.62 m s^{-1}.

Fig. 13d, e, and f illustrate the coordination number, representing the average number of other particles in contact with one particle as a function of the passively vibrated sweep tool displacement. Significant differences were observed in the coordination numbers of the initial particle assemblies. Specifically, assemblies (A), (B), and (C) had coordination numbers of 4.88, 9.63, and 9.55, respectively.

In assemblies consisting of clumps, there was a substantial decrease in the coordination number. In assembly (B) (Fig. 13e), this difference became significant even within the first few millimetres, while in assembly (C) (Fig. 13f), the difference increased with the sweep tool's displacement. This change in the coordination numbers indicated alterations in the interaction patterns between the particles, which were influenced by the sweep tool's geometry and the particle arrangement in the assemblies.

Fig. 14 illustrates noticeable differences in the size and spatial evolution of particle velocities within various particle assemblies as the sweep tool's DEM model moved with a configuration of 16 springs. These disparities were attributed to the distinct textures of the particle assemblies, leading to the formation of deformation zones of varying shapes based on particle geometries. Following the earlier simulations, particle assembly (C) was chosen for further, more detailed kinetic energy simulation studies.

The velocity of the calibrated soil simulated in DEM with assembly (C) is illustrated in Fig. 15, where the subfigures indicated the compacted zone formed during the tillage process, which in this case is shown by displaying the particles moving at a speed of 0.2–0.7 m s^{-1}. Particles that have not entered the specific speed range were hidden in Fig. 15. The difference in the shape of the compacted zone is indicated with red ellipse on each subfigure, which becomes smaller in Fig. 15b due to slips within the particle assembly and was the result of an increase in kinetic energy near the passively vibrated sweep tool's eigenfrequency. From this result it can be clearly seen that due to the vibration of the sweep tool, the volume of the particle assembly set in motion decreased, which in practise allowed a lower mass of soil to be disturbed, thus reducing the amount of the required draught force.

3.5. The results of the developed DEM model of soil and a passively vibrating sweep

3.5.1. Draught force results in assembly C with the corrected geometry

In the final simulations, all other parameters remained constant,

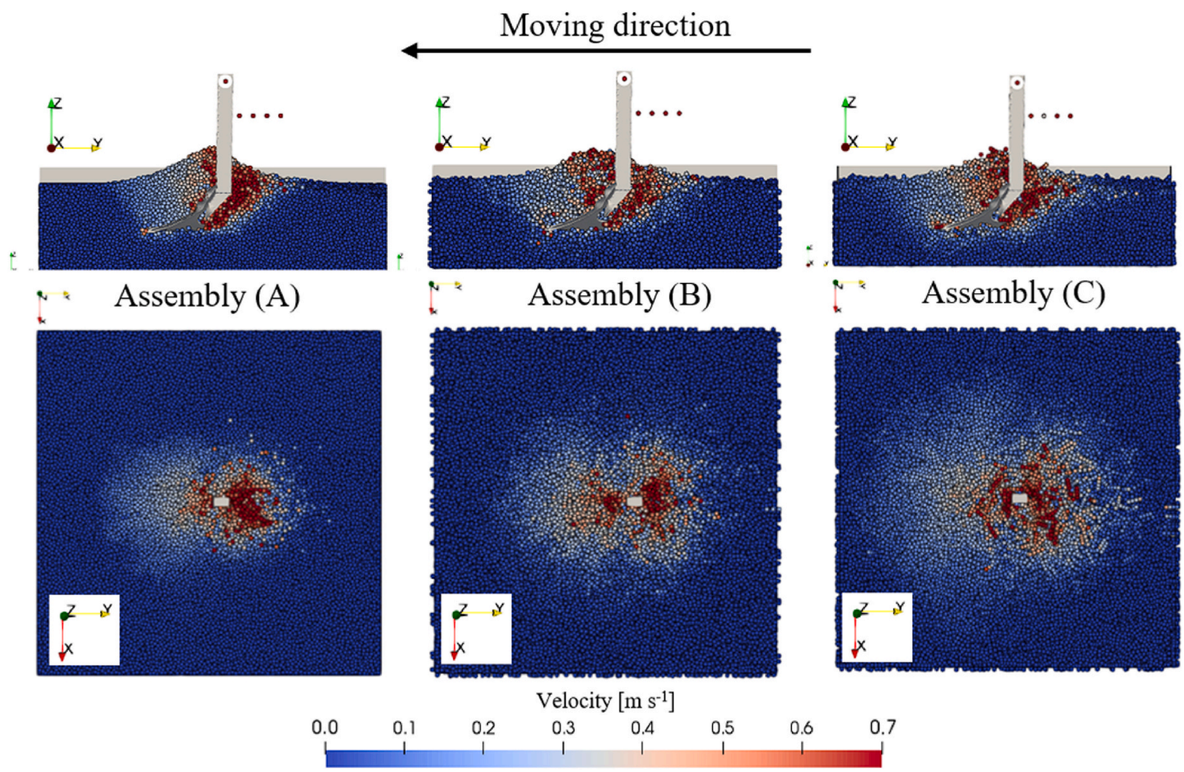

Fig. 14. Velocity of the investigated particle assemblies in case of passively vibrated sweep tool with 16 springs.

except for a modification in the magnitude of the backward bending of the sweep tool model. This alteration was achieved by adjusting the position of the particles representing the spring in the horizontal direction. A negative sign indicated movement in the direction of the tool, while a positive sign signified movement opposite to the tool's direction (Table 2). The position of the particle at the centre of rotation of the passively vibrated sweep tool, crucial for holding and moving the tool, remained consistent with the original configuration. The data from the measurements were incorporated into this setup.

The DEM simulation results closely aligned with the findings from the laboratory soil bin test (Fig. 16). However, a slightly larger fluctuation in the simulated draught force was observable, probably due to the utilisation of particles larger than the actual soil's particle size. Overall, the simulation results provided a close approximation of the results of the empirical measurements, enabling a more precise understanding of the phenomenon under investigation. It is important to note that observed differences could stem from the varying test lengths (20 m in the laboratory compared to the 2 m displacement in DEM simulations) due to computational resource limitations. However, the simulation results remained comparable within these limitations and initial conditions. A potential solution to this limitation in the near future could involve leveraging GPU (Graphics Processing Unit) graphics card acceleration, enabling the use of smaller-sized particles in the millions with realistic computation times (Kalmár et al., 2023; Nagy et al., 2022).

3.5.2. FFT results of the final DEM model

After performing FFT analyses, the simulation results corroborated some phenomena observed in the FFT analyses of the laboratory soil bin measurements. Specifically, when the passively vibrating tool was employed, there was a decrease in the proportion of higher frequencies above 10 Hz, indicating movements and displacements within the particle assembly (Fig. 17).

Based on the DEM simulations, it can be concluded that the FFT calculated from the draught force of the simulated rigid and passively vibrating sweep tool behaved similarly to the laboratory measurement results from the soil bin study. This similarity confirmed the suitability of the developed DEM model for analysing the investigated physical phenomena. The most significant decrease in the simulated draught force occurred in the DEM model for those spring configurations of the sweep tool where the larger draught force amplitudes were reduced to the range below 10 Hz in the case of the passively vibrating sweep tool (Fig. 17).

The FFT analysis of the displacement of the passively vibrated sweep tool revealed that the 16 spring configuration exhibited the most significant increase in displacement amplitude at frequencies close to or below a specific frequency, with the highest proportion occurring at 8.34 Hz (Fig. 18d). In the most rigid setting with 4 springs, a higher frequency of the sweep tool's vibration was achieved, as expected. This might be caused by the lower inclined angle resulting from the assembled structure of the measurement instrument of the passively vibrated sweep tool (Payne et al., 1959). However, it was observed that in the softest configuration, with 32 springs, additional draught force reduction was still simulated in the DEM model, contrary to the empirically measured results. This inconsistency suggested that further testing and refinement of the developed model is still required.

3.6. The results of energetic properties of the developed DEM model

3.6.1. The results of the sweep tool's kinetic energy

The trend exhibited by the kinetic energy of the passively vibrated sweep tool aligned well with the decrease in draught force compared to the rigid tool (Fig. 19). Additionally, the most significant fluctuation in kinetic energy due to vibration, which was presumably close to the tool's eigenfrequency, was observed when the 16 spring configuration was used (Fig. 19d) and similar to the empirical test results obtained from the real measurement setup.

3.6.2. The results regarding the kinetic energy of the particle assembly

The subfigures of Fig. 20 depict the evolution of the kinetic energy of the entire particle assembly concerning the displacement of the sweep

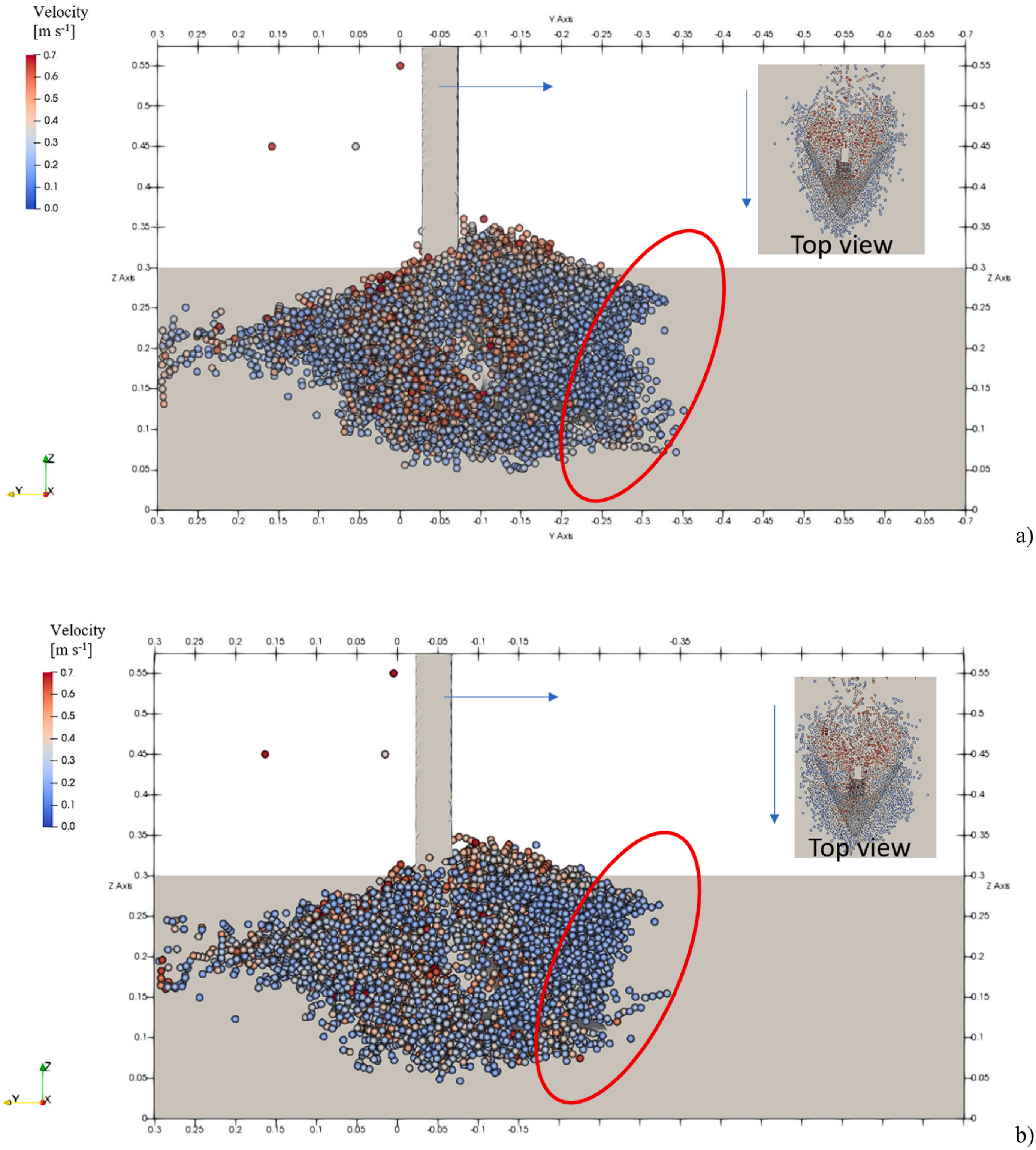

Fig. 15. The velocity in the section view of the calibrated model with a) the rigid sweep tool and b) in case of passively vibrated sweep tool with 16 springs. For a meaningful visualisation, only the particles moving at threshold speeds 0.2–0.7 m s^{-1} were shown in these figures created the compacted zone around the sweep (particles out of this range were hidden). The difference in the same timestep between the size of the resulting compacted zones is indicated by the red ellipses. (The dimension of the axes is in m.) (For interpretation of the references to colour in this figure legend, the reader is referred to the Web version of this article.)

tool. The results were obtained at a displacement of 2 m, where an increase in kinetic energy in the particle assembly was evident. Although the kinetic energy from particle rotation was negligible compared to the longitudinal kinetic energies, using higher numbers of springs, such as 28 and 32 springs, resulted in an increase in the kinetic energy value from the rotational movement of the particles toward the end of the simulations (Fig. 20g and h).

In the results of simulations employing 4, 8, and 16 spring configurations, it was observed that the passively vibrated and rigid tools generated almost identical kinetic energy in the particle assembly, with

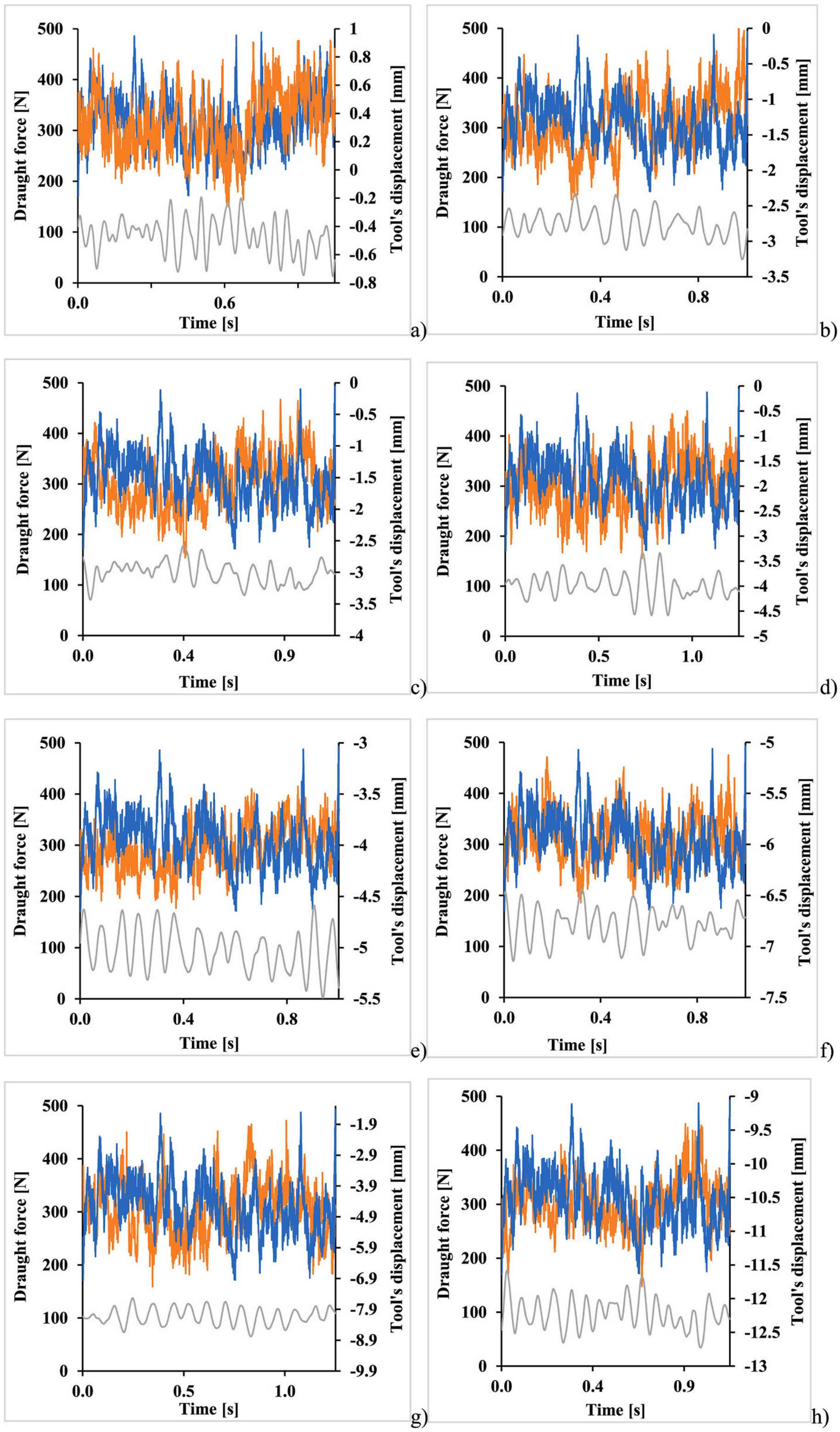

Fig. 16. The simulated draught force of — rigid and — passively vibrated sweep tool and the — tools displacement at the "measured" point (see Fig. 1c) of contact between the spring and the sweep tool's shank utilise a) 4, b) 8, c) 12, d) 16, e) 20, f) 24, g) 28, h) 32 springs.

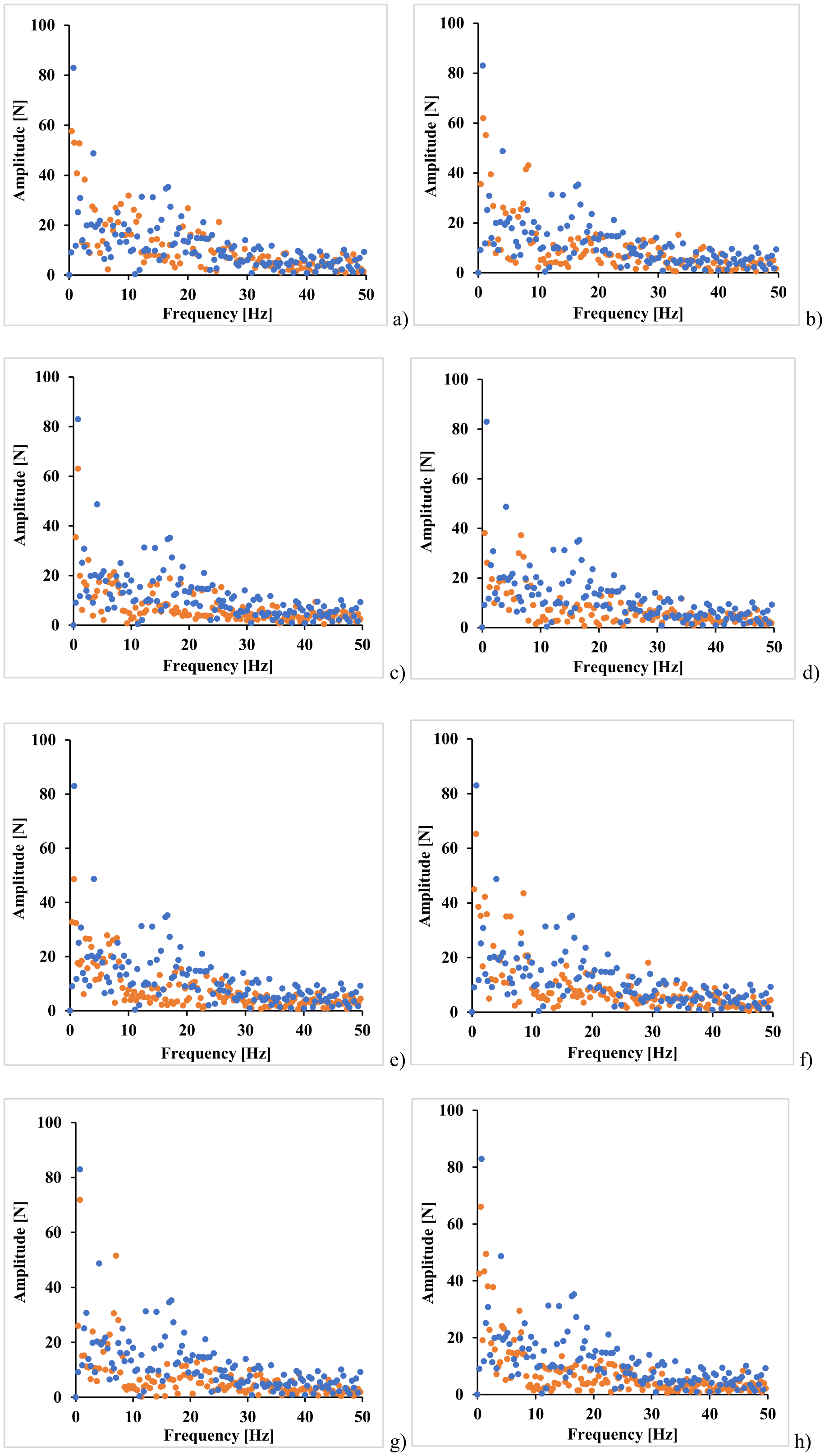

Fig. 17. The results of the FFT of the DEM simulation models on different spring configurations of the rigid tool and the passively vibrated sweep tool, where the configurations of a) 4, b) 8, c) 12, d) 16, e) 20, f) 24, g) 28, h) 32 springs were used.

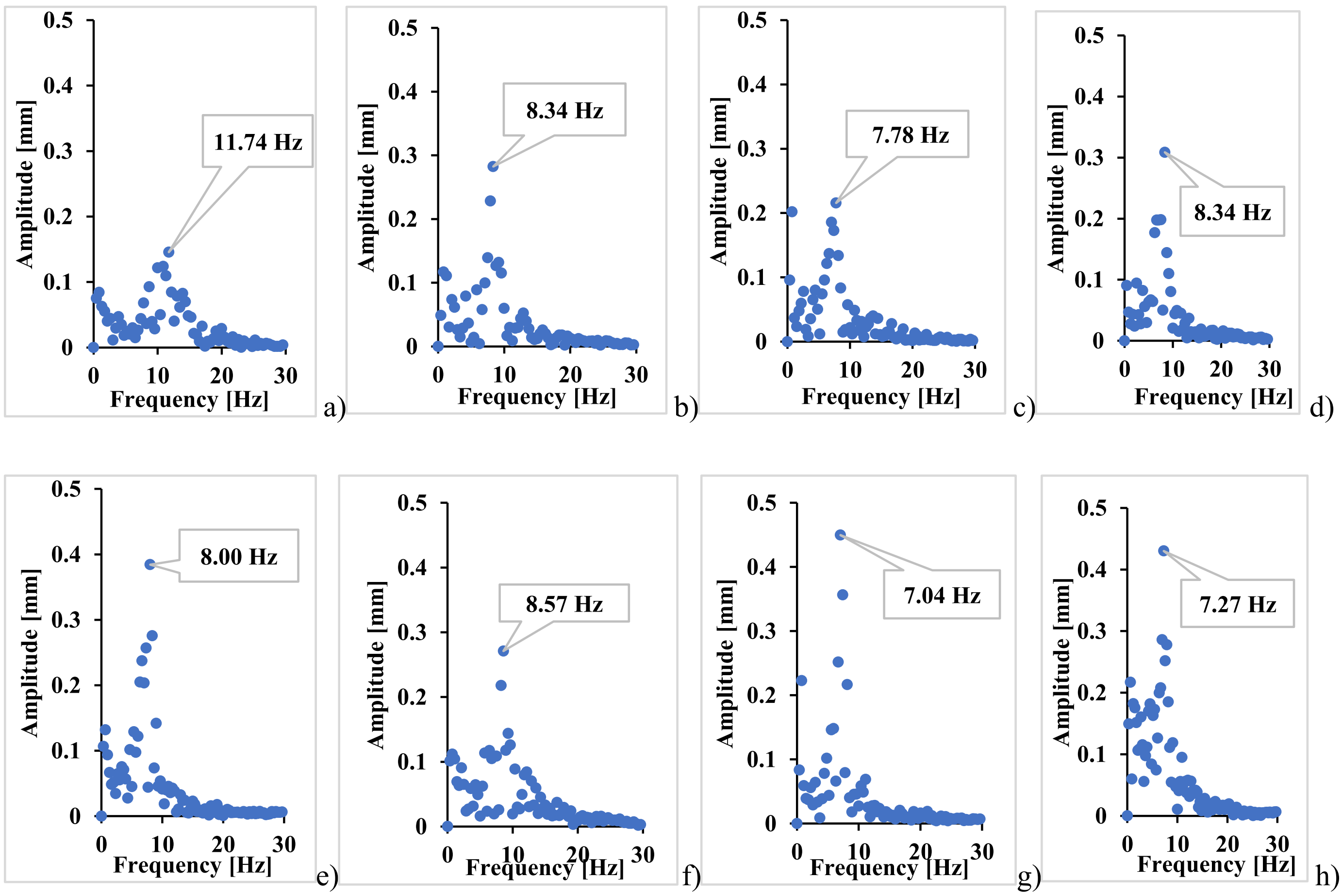

Fig. 18. The FFT analyses of the passively vibrated sweep tool's displacement in DEM, where a) 4, b) 8, c) 12, d) 16, e) 20, f) 24, g) 28, h) 32 springs were used.

the same magnitude. Based on the simulation results of the DEM model of the soil's interaction with the passively vibrated tool, it can be concluded that the draught force was lowest in the model setting where the kinetic energy of the passively vibrated sweep tool was the highest, and the kinetic energy of the particle assembly, indicating the dissipated or generated energy in the particle assembly, was the lowest, where the assembly flows the most easily.

The research results demonstrated that DEM is suitable for analysing the action mechanism of the interaction between the soil and the passively vibrated sweep. Although the model calibrated with the GA mostly produced the expected results, for simulating specific settings as accurately as possible, further calibration of the model will be required for additional geometries and soil types.

4. Discussion

This research clearly demonstrated that towing a sweep tool, which is supported by an appropriate spring configuration, requires the use of a lower draught force compared to a rigid tool. A configuration with 16 springs showed a reduction in the draught of almost 6–9% in both an empirical soil bin test and a DEM simulation, where a considerably higher damping coefficient (<0.2) was observed at a given frequency in comparison with the other spring configurations damping factors (<0.1). A further slight reduction in the draught force required was observed when a 24 spring configuration was employed, although the larger number of springs increased the degree of compression, causing the sweep tool to bend back more and thus creating a different contact geometry with the soil. Based on the laboratory soil bin test, this decrease was explained by the movement of the sweep tool at a lower distance, hence it is not in constant contact with the soil. As a result, additional energy was generated due to the operation being close to the passively-vibrating sweep tool's eigenfrequency. However, the interaction of soil with a passively-vibrating sweep could not be analysed from an energy point of view by analysing the measurement results alone, therefore a sufficiently precisely adjusted DEM model was used, allowing a more detailed analysis of the real physical phenomenon.

Based on the GA calibrated DEM simulation results, it was possible to produce an RE of less than 0.1% between the actual measurement and the DEM, which was also supported by the results of FFT and direct shear box tests. In contrast to the previous so-called manual calibration methods, the calibration of the DEM model was achieved with a high level of accuracy. This played an important role in the methodology developed in this research, since in this very complex task, even in relation to the variables used in this model, several suitable parameter combinations can provide an appropriate solution when calibration procedures are based on specific measurements.

Using GA, the geometric structure of the DEM model and the micromechanical parameters utilised in the contact model should be set based on the results of previous experiments with appropriate simplifications. This research clearly highlighted the right choice of particle shape for approximating soil structure in a DEM model. The target value to be achieved should also be set based on preliminary results, because the GA can learn any predefined value with high precision. The application of the 3D scanned tool geometry as a free body model in the simulation allowed an accurate description of the tool's geometry and its inertia moment to reproduce the real phenomenon in the DEM model accurately, so even the effect of tool wear on its vibration in the soil can be analysed. Unlike the harmonic motion engine utilised in previous studies, which produced infinitely large energy within the system and did not work synchronously when model soil failures occurred, the

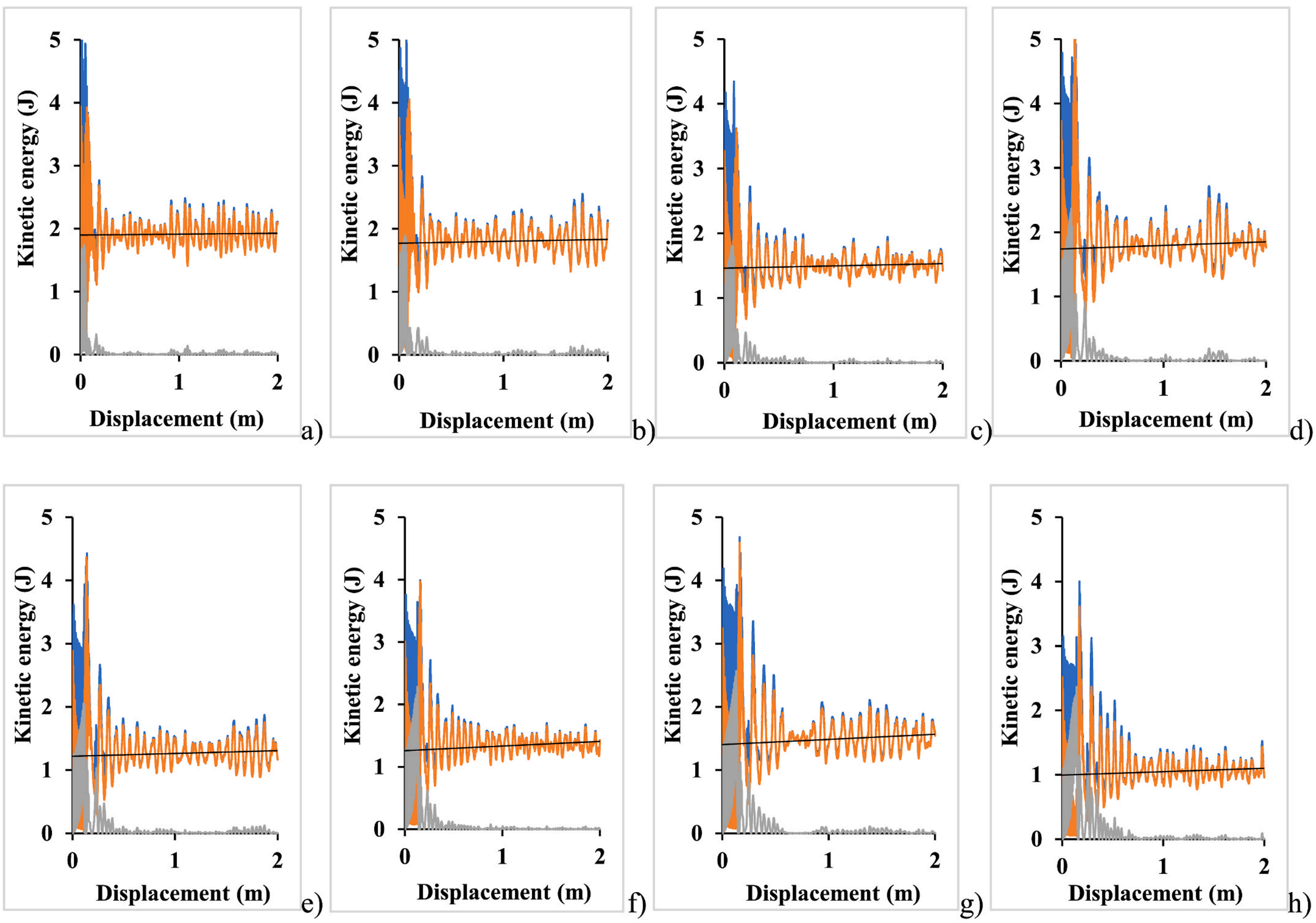

Fig. 19. The results of the passively vibrated sweep's DEM model kinetic energy and the equation of the trend line, with different number of springs: a) 4 (y = 0.0148x+1.8979), b) 8 (y = 0.0298x+1.7718), c) 12 (y = 0.0347x+1.4608), d) 16 (y = 0.0562x+1.7386), e) 20 (y = 0.0448x+1.2183), f) 24 (y = 0.0742x+1.2593), g) 28 (y = 0.0807x+1.4043), h) 32 (y = 0.0528x+0.994). (total kinetic energy, kinetic energy from transversal, kinetic energy from rotational movement).

sweep tool's free body model allowed the individual study of the kinetic energy of each element in the entire system and to model how the tool's vibration works synchronously with cracks in the soil. It should be noted, however, that using GA in the calibration procedure was not intended to accelerate the process, but rather to automate it, hence, by optimally searching, it can find parameter sets that the user may not be able to find with manual calibration methods.

Meanwhile, the duration of the calibration process depended largely on the level of development of the DEM model created. Nowadays, increased speed of GPUs and parallel running simulation techniques can significantly reduce the calibration time required for GA. Furthermore, it should not be overlooked that the results of DEM and GA runs can be archived and form the basis for future artificial intelligence applications, that may allow engineers to solve this calibration problem in only a few seconds with the help of the existing data set.

5. Conclusions

This study analysed the experimental results from a sweep tool designed for passive vibration in a laboratory soil bin. Comparative tests were conducted with a DEM model using particle assemblies with varied geometries. The main novelty value of this study lies in simulating a passively vibrated sweep tool that actually vibrates by a discrete element method soil model calibrated with a genetic algorithm. Unlike real measurements, this simulation allowed for an in-depth study of the kinetic energy of both the sweep and the particle assembly during its operation. Based on this research, the following conclusions can be drawn:

In the DEM model, in addition to the particle assembly, the sweep can be simulated as a free body by adjusting its inertia and implementing appropriate constraints and initial conditions. This enables the accurate simulation of the passively vibrating sweep tool within the DEM framework.

Based on the calibration procedure, it can be stated that, during the calibration of the DEM model of the interaction between the soil and the passively vibrated sweep tool, the texture formed in the particle assembly containing 90% elongated particle shapes, in addition to the micromechanical parameter set governing particle interactions, proved to be crucial for accurately mapping the fundamental physical phenomena in the DEM model.

When a 16 spring configuration of the sweep tool was studied, both in the soil bin study and in the DEM model calibrated precisely through genetic algorithms, a significant reduction in draught force was observed. This reduction can be attributed to a substantial increase in the kinetic energy of the passively vibrated sweep tool, resulting in reduced energy dissipation within the particle assembly of the DEM model of the soil. This phenomenon stems from the amplified vibration acceleration of the sweep tool.

The frequency and damping coefficient of the passively vibrating sweep tool, along with the micromechanical parameters of the particle

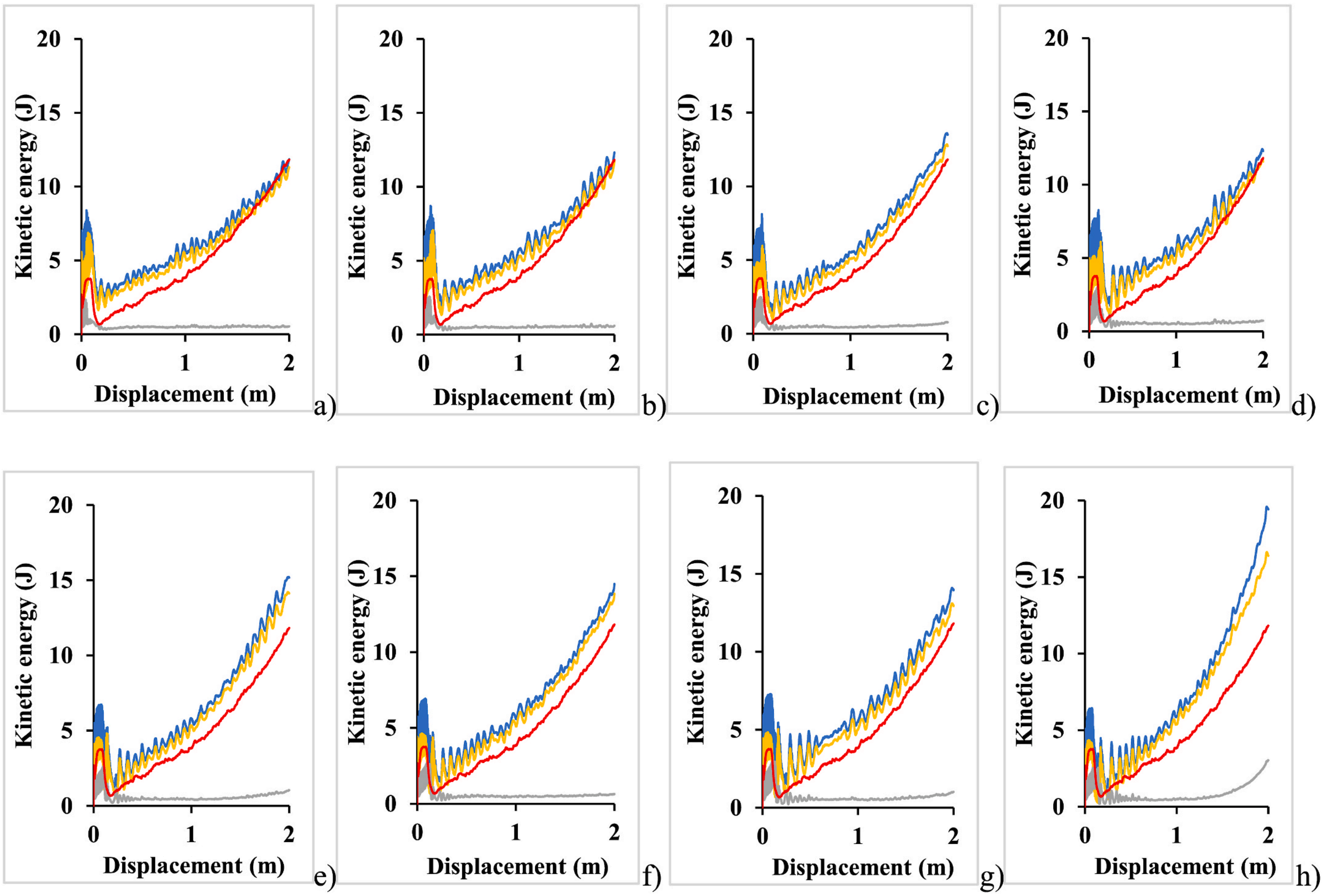

Fig. 20. The kinetic energy of the particle assembly (C), where a) 4, b) 8, c) 12, d) 16, e) 20, f) 24, g) 28, h) 32 springs. (— total kinetic energy, — kinetic energy from transversal, — kinetic energy from rotational movement, — total kinetic energy for a rigid sweep tool).

assembly, were accurately adjusted using PYGAD genetic algorithm software. However, it is worth noting that multiple combinations of parameters were suitable for modelling the draught force during the soil model calibration. The most relevant parameter set for the actual soil conditions was selected using direct shear box simulations.

Utilising the FFT, it became possible to discern the frequency proportions in the draught force and the passively vibrated sweep tool's displacement, both in the model and simulation.

In conclusion, these simulation studies suggest that if spring stiffness and damping factor are taken into consideration as variables, the optimal parameter settings for the passively vibrated sweep tool can be determined from the initial data. This determination is achievable by setting the minimum draught force as the target, as per the fitness function of the genetic algorithm. The initial data capture the mechanical properties of the investigated soil and the geometrical and mass conditions of the employed tillage tool.

CRediT authorship contribution statement

Kornél Tamás: Writing – review & editing, Writing – original draft, Visualization, Validation, Software, Resources, Project administration, Methodology, Investigation, Funding acquisition, Formal analysis, Data curation, Conceptualization.

Declaration of competing interest

The authors declare that they have no known competing financial interests or personal relationships that could have appeared to influence the work reported in this paper.

Acknowledgement

The author gratefully acknowledge the assistance of the staff at the Institute of Technology of the Hungarian University of Agriculture and Life Sciences for allowing the use of their testing facilities and for providing practical support while the measurements were being carried out. Special thanks are due to Zoltán Hudoba for his support during the experiments. This paper was supported by the János Bolyai Research Scholarship of the Hungarian Academy of Sciences. The research reported in this paper is part of project no. TKP-6-6/PALY-2021, implemented with the support provided by the Ministry of Innovation and Technology of Hungary from the National Research, Development and Innovation Fund, financed under the TKP2021-NVA funding scheme. This research was supported by the ÚNKP, funded by the National Research Development and Innovation Fund under grant number ÚNKP-23-5-BME-80. This paper was supported by the Hungarian Scientific Research Fund (NKFIH FK-146067).

References

Ai, J., Chen, J. F., Rotter, J. M., & Ooi, J. Y. (2011). Assessment of rolling resistance models in discrete element simulations. *Powder Technology, 206*(3), 269–282.

Bandalan, E. P., Salokhe, V. M., Gupta, C. P., & Niyamapa, T. (1999). Performance of an oscillating subsoiler in breaking a hardpan. *Journal of Terramechanics, 36*(2), 117–125.

Barbosa, L. A. P., Gerke, K. M., Munkholm, L. J., Keller, T., & Gerke, H. H. (2022). Discrete element modeling of aggregate shape and internal structure effects on

Weibull distribution of tensile strength. *Soil and Tillage Research, 219*, Article 105341.
Chen, Y., Munkholm, L. J., & Nyord, T. (2013). A discrete element model for soil–sweep interaction in three different soils. *Soil and Tillage Research, 126*, 34–41.
Cundall, P. A. (1971). A computer model for simulating progressive, large-scale movement in blocky rock system. *Proceedings of the International Symposium on Rock mechanics, 8*, 129–136.
Cundall, P. A., & Strack, O. D. (1979). A discrete numerical model for granular assemblies. *Géotechnique, 29*(1), 47–65.
Dubrovskii, A. A. (1956). Influence of vibrating the tools of cultivating implements upon draft resistance. *National Institute of Agricultural Engineering Translation*, (51).
Dzhabborov, N., Dobrinov, A., & Sergeev, A. (2021). Vibration parameters and indicators of a dynamic tillage tool. In *IOP Conference series: Earth and Environmental Science, 937*IOP Publishing, Article 032048. No. 3.
Eggenmüller, A. (1958). Oscillating implements: Kinematics and experiments with model. *Grundlagen der Landtechnik, 10*, 55–69.
Fenyvesi, L., & Hudoba, Z. (2010). Vibrating tillage tools. *Soil Engineering*, 31–49.
Fenyvesi, L., Jóri, I. J., & Borsa, B. (2002). Reduction of the energy requirement by new soil cultivation tools. In *2002 ASAE Annual Meeting Proceedings* (p. 1). American Society of Agricultural and Biological Engineers.
Foldager, F. F., Munkholm, L. J., Balling, O., Serban, R., Negrut, D., Heck, R. J., & Green, O. (2022). Modeling soil aggregate fracture using the discrete element method. *Soil and Tillage Research, 218*, Article 105295.
Gad, A. F. (2021). *Pygad: An intuitive genetic algorithm python library*. arXiv preprint arXiv: 2106.06158.
Gunn, J. T., & Tramontini, V. N. (1955). Oscillation of tillage implements. *Agricultural Engineering, 36*(11), 725–729.
Hendrick, J., & Buchele, W. (1963). Tillage energy of a vibrating tillage tool. *Transactions of the ASAE, 6*(3), 213–216.
Holmes, M. A. J., Brown, R., Wauters, P. A. L., Lavery, N. P., & Brown, S. G. R. (2016). Bending and twisting friction models in soft-sphere discrete element simulations for static and dynamic problems. *Applied Mathematical Modelling, 40*(5–6), 3655–3670.
Horváth, D., Poós, T., & Tamás, K. (2019). Modeling the movement of hulled millet in agitated drum dryer with discrete element method. *Computers and Electronics in Agriculture, 162*, 254–268.
Kalmár, P., Hegedűs, F., Nagy, D., Sándor, L., & Klapcsik, K. (2023). Memory-friendly fixed-point iteration method for nonlinear surface mode oscillations of acoustically driven bubbles: From the perspective of high-performance GPU programming. *Ultrasonics Sonochemistry, 99*, Article 106546.
Karmakar, S., Kushwaha, R. L., & Stilling, D. S. D. (2005). Soil failure associated with crack propagation for an agricultural tillage tool. *Soil and Tillage Research, 84*(2), 119–126.
Keppler, I., Hudoba, Z., Oldal, I., Csatár, A., & Fenyvesi, L. (2015). Discrete element modeling of vibrating tillage tools. *Engineering Computations, 32*(2), 308–328.
Kofoed, S. S. (1969). Kinematics and power requirement of oscillating tillage tools. *Journal of Agricultural Engineering Research, 14*(1), 54–73.
Meola, A., Winkler, M., & Weinrich, S. (2023). Metaheuristic optimization of data preparation and machine learning hyperparameters for prediction of dynamic methane production. *Bioresource Technology, 372*, Article 128604.
Nagy, D., Plavecz, L., & Hegedűs, F. (2022). The art of solving a large number of non-stiff, low-dimensional ordinary differential equation systems on GPUs and CPUs. *Communications in Nonlinear Science and Numerical Simulation, 112*, Article 106521.
Oladapo, A. O. (1993). *Investigation of a plough's natural frequency effect on tillage forces in a sandy loam soil. Doctoral dissertation*. University of South Australia.
Ono, I., Nakashima, H., Shimizu, H., Miyasaka, J., & Ohdoi, K. (2013). Investigation of elemental shape for 3D DEM modeling of interaction between soil and a narrow cutting tool. *Journal of Terramechanics, 50*(4), 265–276.
Pásthy, L., Farkas, Z. J., Haba, T., & Tamás, K. (2024). Development of a multi-way coupled discrete-finite element method simulation procedure for modelling soil-passive vibration tool interaction. *Computers and Electronics in Agriculture, 216*, Article 108459.
Payne, P. C. J., & Tanner, D. W. (1959). The relationship between rake angle and the performance of simple cultivation implements. *Journal of Agricultural Engineering Research, 4*(4), 312–325.
Roessler, T., Richter, C., Katterfeld, A., & Will, F. (2019). Development of a standard calibration procedure for the DEM parameters of cohesionless bulk materials–part I: Solving the problem of ambiguous parameter combinations. *Powder Technology, 343*, 803–812.
Sadek, M. A., Chen, Y., & Liu, J. (2011). Simulating shear behavior of a sandy soil under different soil conditions. *Journal of Terramechanics, 48*(6), 451–458.
Shahgoli, G., Fielke, J., Desbiolles, J., & Saunders, C. (2010). Optimising oscillation frequency in oscillatory tillage. *Soil and Tillage Research, 106*(2), 202–210.
Šmilauer, V., & Chareyre, B. (2010). Yade dem formulation. *Yade Documentation, 393*.
Šmilauer, V., Chareyre, B., Duriez, J., Eulitz, A., Gladky, A., Guo, N., … Kozicki, J. (2015). *Using and Programming, yade Documentation*.
Smilauer, V., et al. (2015). *Yade Documentation* (2nd ed.). https://doi.org/10.5281/zenodo.34073 http://yade-dem.org
Soeharsono, P., & Setiawan, R. A. (2010). Analytical study of self-excited vibration on single degree of freedom vibratory-tillage. *ARPN Journal of Engineering and Applied Sciences, 5*(9), 61–66.
Sulatisky, M. T., & Ukrainetz, P. R. (1972). Draft reduction by vibratory soil cutting. *Transactions of the Canadian Society for Mechanical Engineering, 1*(4), 175–181.
Tamás, K. (2018). The role of bond and damping in the discrete element model of soil-sweep interaction. *Biosystems Engineering, 169*, 57–70.
Tamás, K., & Bernon, L. (2021). Role of particle shape and plant roots in the discrete element model of soil–sweep interaction. *Biosystems Engineering, 211*, 77–96.
Tekeste, M. Z., Balvanz, L. R., Hatfield, J. L., & Ghorbani, S. (2019). Discrete element modeling of cultivator sweep-to-soil interaction: Worn and hardened edges effects on soil-tool forces and soil flow. *Journal of Terramechanics, 82*, 1–11.
Ucgul, M., Fielke, J. M., & Saunders, C. (2014). 3D DEM tillage simulation: Validation of a hysteretic spring (plastic) contact model for a sweep tool operating in a cohesionless soil. Soil *and Tillage Research. 144*, 220–227.
Ucgul, M., Fielke, J. M., & Saunders, C. (2015). Three-dimensional discrete element modelling (DEM) of tillage: Accounting for soil cohesion and adhesion. *Biosystems Engineering, 129*, 298–306.
Upadhyaya, S. K., Ma, T. X., Chancellor, W. J., & Zhao, Y. M. (1987). Dynamics of soil—tool interaction. *Soil and Tillage Research, 9*(2), 187–206.
Van der Linde, J. (2007). *Discrete element modeling of a vibratory subsoiler*. Doctoral dissertation. Stellenbosch: University of Stellenbosch.
Wensrich, C. M., & Katterfeld, A. (2012). Rolling friction as a technique for modelling particle shape in DEM. *Powder Technology, 217*, 409–417.
Xirui, Z., Chao, W., Zhishui, C., & Zhiwei, Z. (2016). Design and experiment of a bionic vibratory subsoiler for banana fields in southern China. *International Journal of Agricultural and Biological Engineering, 9*(6), 75–83.
Yow, J., & Smith, J. L. (1976). Sinusoidal vibratory tillage. *Journal of Terramechanics, 13*(4), 211–226.
Zhang, J. (1997). *Vibratory analysis of tillage operation*. Doctoral dissertation. University of Saskatchewan).
Zhu, M. (2021). *Genetic algorithm-based parameter Identification for Ship Manoeuvring model under Wind disturbance. Master's thesis*. Norwegian University of Science and Technology.